This document is currently under revision by the European Commission (EC) and has not yet been validated or approved by the EC. The content provided herein is subject to change, and the information presented may not represent the final position or official stance of the EC.

This document is being shared for informational purposes only and is not to be considered an official or authoritative source of information from the European Commission. Any decisions, actions, or interpretations based on the content of this document should be taken with caution, as the content may be subject to modification or revision by the EC.

The EC accepts no liability for any inaccuracies, errors, or omissions in this document, and any reliance on its content is at the user's own risk. It is recommended to verify the information provided in this document with official EC publications or communications before making any decisions or drawing any conclusions based on its content.

Please note that the content in this document may be confidential or sensitive in nature and should be treated as such. Unauthorized dissemination, distribution, or use of this document is strictly prohibited.

By accessing and reviewing this document, you acknowledge and accept the terms of this disclaimer.

BL2F

Transforming Black Liquor to Biofuel

Research and Innovation Action

H2020-LC-SC3-2019-NZE-RES-CC

D3.5 - Report on HDO kinetic modelling

WP3 - Task 3.4 Modelling of HDO processes

26.3.2024

Lead Beneficiary: VTT

Author(s): Kristian Chen (VTT), Juha Lehtonen (VTT)

@BL2F_EU **www.bl2f.eu** **BL2F_EU**

This project has received funding from the European Union's Horizon 2020 research and innovation programme under the Grant Agreement n°884111.

Disclaimer

The content of this deliverable reflects only the author's view. The European Commission is not responsible for any use that may be made of the information it contains.

Document Information

Grant agreement	884111
Project title	Black Liquor to Fuel by Efficient Hydrothermal Application integrated to Pulp Mill
Project acronym	BL2F
Project coordinator	Prof. Dr. Tero Joronen
Project duration	1st April 2020 – 31st March, 2024 (48 Months)
Related work package	WP 3 - Upgrading and application testing
Related task(s)	Task 3.4 - Modelling of HDO processes
Lead organisation	VTT
Contributing partner(s)	-
Due date	31.3.2024
Submission date	26.3.2024
Dissemination level	Public

History

Date	Version	Submitted by	Reviewed by	Comments
26.3.2024	1.0	Kristian Chen	Juha Lehtonen, Sari Rautiainen	

Table of contents

List of figures

Abbreviations and acronyms

Acronym	Description
HDO	Hydrodeoxygenation
IHDO	Integrated hydrodeoxygenation
HTL	Hydrothermal liquefaction
TOF	Turnover frequency
HYD	Hydrogenation
DDO	Direct deoxygenation
ACI	Acid-catalyzed
AC	Activated carbon
ODE	Ordinary differential equation
EP	2-ethylphenol
EB	2-ethylbenzene
DHEP	dihydro-ethylphenol
ECHE	ethylcyclohexene
ECH	ethylcyclohexane
DHBF	2,3 dihydrobenzofuran
BF	Benzofuran
ECHOH	Ethylcyclohexanol
NPs@IP	Nanoparticle catalysts stabilized with ether-functionalized ionic polymer

Executive Summary

In this report the kinetics of both hydrothermal and non-hydrothermal HDO were discussed by reviewing existing literature. Various proposed reaction networks were presented and some of the methodologies used for evaluating kinetic parameters were also presented. The reaction networks were mostly for model components, which were phenol compounds and benzofuran. Reaction networks derived from real oils were also presented, however the very limited research on this made it possible to only give a couple of examples. The reaction networks of model components in non-hydrothermal HDO were compared to their counterparts in hydrothermal HDO to evaluate the effect that hydrothermal conditions have on the kinetics of HDO.

The main products of hydrothermal HDO of phenols are cycloalkanes and cycloalkanols. The reaction generally begins with the hydrogenation of the aromatic ring, except when no acid was used alongside the catalyst, in which case the hydrogenation of the aromatic ring happens later in the reaction. There also seem to be some steps in the reaction which are catalyzed by acid instead of the metal catalyst. The last steps of the reaction where cycloalkanes are formed are temperature dependent, where the amount of cycloalkanes produced decreases drastically when below a certain temperature. The calculated values for the activation energies for the different reaction steps can range from 30 $\frac{kJ}{mol}$ up to 150 $\frac{kJ}{mol}$. The hydrothermal HDO of benzofuran produces both cycloalkanes and benzenes.

Comparing the reaction networks proposed for non-hydrothermal/aqueous-phase HDO with hydrothermal/aqueous-phase HDO, most of them are structurally similar with the main differences being the intermediate products. It is unclear how exactly the hydrothermal/aqueous-phase environment affects the kinetics of HDO, since even in comparable studies there were always other factors that also could have affected the results of the experiment, such as a slightly different catalyst/support or a difference in hydrogen pressure. Additionally, since the reaction networks were mainly formed by using model compounds, their accuracy might be limited when applied to the HDO of real oils. Based on this current report, it seems that the choice of catalyst has a larger effect on the reaction network of HDO compared to a hydrothermal environment.

Keywords

Black liquor, Hydrodeoxygenation, Kinetics, Heterogeneous catalysis

1 Introduction

The focus of the BL2F project has been to develop an integrated concept for hydrothermal liquefaction of black liquor from Kraft pulp mills and upgrading of the HTL biocrude to transportation fuels. The upgrading will be performed by a two stage hydrodeoxygenation (HDO) process of which the first stage hydrothermal hydrodeoxygenation is integrated to the pulp mill (IHDO) and the second stage is supposed to be integrated e.g. to an oil refinery. BL2F concept is presented in Figure 1.

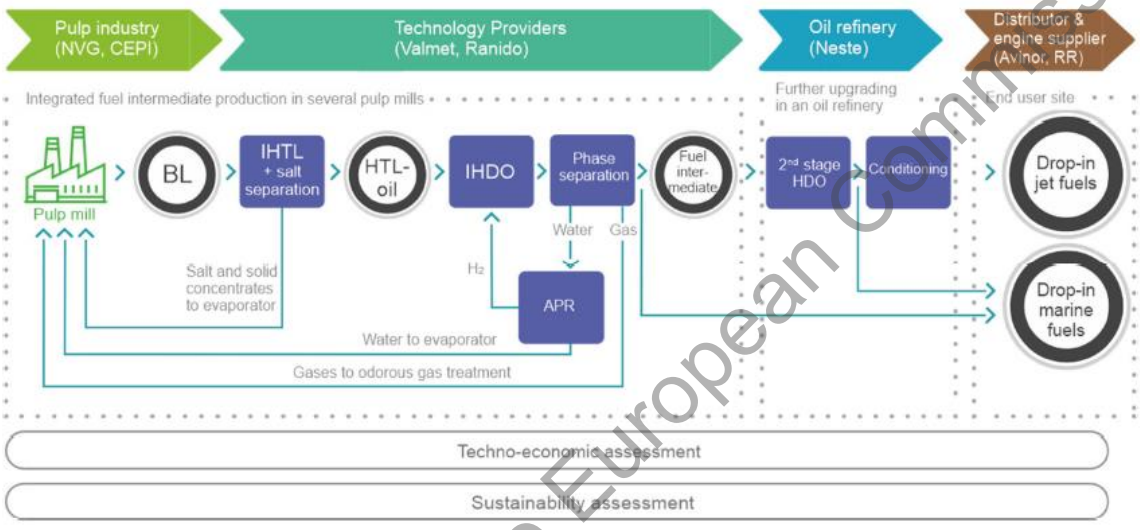

Figure 1. Overview of the BL2F process.

The original focus of Task 3.4 of the BL2F project was to determine reaction kinetics of both HDO stages based on the data from kinetic experiments performed as a part of the project and apply the developed kinetic models for the simulation of BL2F concept and for the process scale up purposes. However, due to lack of black liquor based HTL biocrude to be applied for the experiments, it was not possible to determine reaction kinetics for neither of the HDO stages. Instead of the original objective, the focus of the task was decided to be to perform a literature review on the kinetics of bio-oils and bio-oils model compounds HDO. The findings of this study are reviewed in this report.

2 Kinetics of the bio-oils hydrodeoxygenation process

Since there is very limited information on the kinetics of hydrothermal HDO of bio-oils, for this report, the HDO process is considered to be hydrothermal if the reaction happens in the presence of an aqueous phase. It has been claimed that there are some benefits to perform HDO hydrothermally near critical or supercritical conditions. Water offers better product separation for water-insoluble alkanes and may improve the hydrogenation of certain compounds (Zhao et al., 2009). Supercritical water readily dissolves organic compounds forming one homogeneous phase (Liu et al., 2022). As a medium, supercritical water has a high diffusion rate and low mass transfer limitations which usually provide high reaction rates for heterogeneous catalysis (Kruse & Dinjus, 2007). Additionally, coke formation is limited and may be prevented (Kruse & Dinjus, 2007). There is also some evidence, which suggests that water directly improves the HDO process by for example increasing the selectivity of the hydrogenated and deoxygenated products as well as conversion (Nelson et al., 2015). From a process design standpoint, since the aqueous portion of the feed would require less pre-processing, more of the oil can be utilized with less waste treatment (Dickinson et al., 2012).

In this work, the kinetics of both hydrothermal and non-hydrothermal HDO are discussed. The kinetics are mainly discussed through reviewing proposed reaction networks and pathways in various studies, and if kinetic parameters have been evaluated, the methodologies used for the calculations are also presented.

2.1 Hydrothermal HDO

There is limited research done on the kinetics of hydrothermal HDO. In most cases, model components are used instead of real oils. These model components mostly consist of phenols (Saidi & Safaripour, 2022; Yang et al., 2014; Yu, Wang, Liu, et al., 2018; Yu, Wang, Sun, et al., 2018; Zhang et al., 2016; Zhao et al., 2011). Additionally, some studies discuss the use of benzofurans (Dickinson et al., 2012).

2.1.1 Hydrothermal HDO of real oils

Sanna et al. (2015) studied the kinetics of the aqueous phase HDO of real bio-oils. Bio-oil made by the fast pyrolysis of dry pine wood was separated into its water-soluble fraction and the insoluble fraction. The water-soluble fraction of the bio-oil was used in the HDO. The experiments were done in either a one-stage or a two-stage reactor setup where two reactors were in a series. The reactors were continuous flow packed bed reactors. Low and high temperature HDO was studied by using a temperature range of 348 – 523 K. Ru/C and Pt/C were used as the catalysts. The authors propose a reaction network for the HDO of bio-oils which is shown in Figure 2. There were four different reaction types that were identified by Sanna et al. (2015) presented in the figure. The first one is the primary hydrogenation of

carbonyl groups at low temperature to corresponding alcohols, the second one is the hydrolysis of levoglucosan C-O-C bonds to glucose in the presence of acid cites, the third are the hydrogenolysis reactions of polyols with C-C bond cleavage, and the last ones are the secondary hydrogenation reactions catalysed by the metal to produce monohydric alcohols from diols.

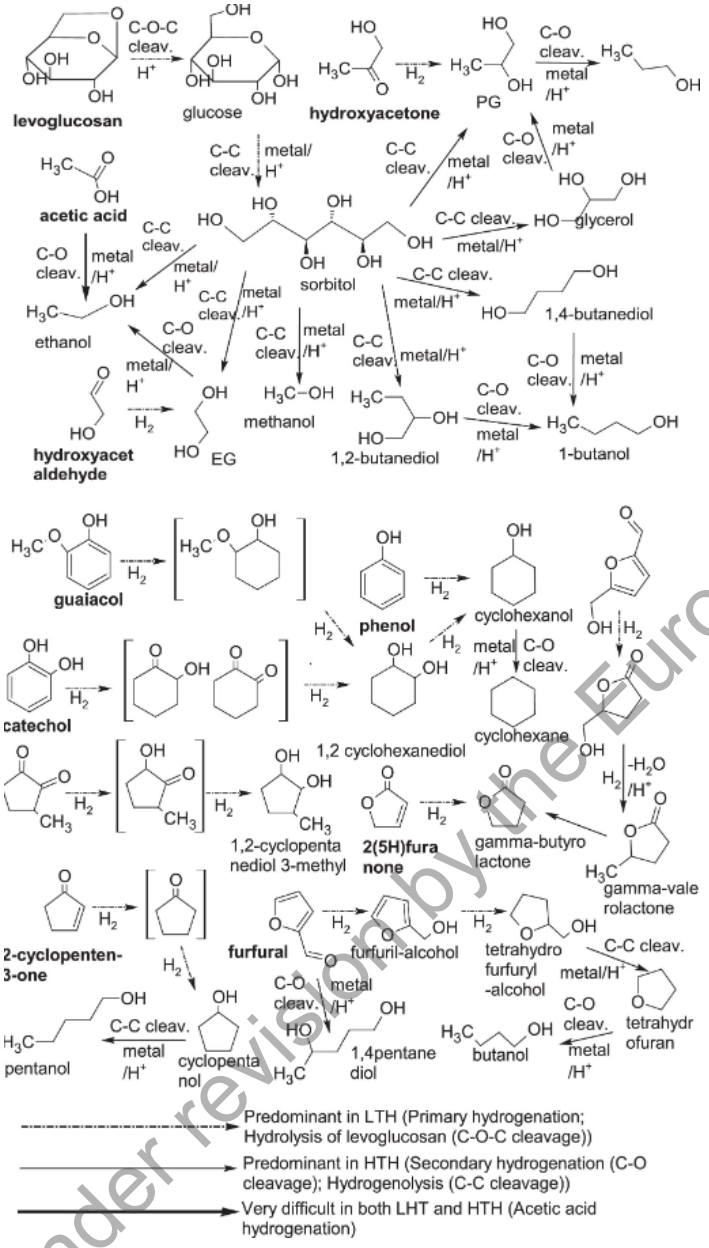

Figure 2. Proposed reactions for the HDO of bio-oils. The reactants are bolded and the intermediates are enclosed in []-brackets. (Sanna et al., 2015)

2.1.2 Hydrothermal HDO of phenols

Zhao et al. (2011) studied the kinetics of phenol, anisole, catechol and guaiacol on a Pd/C catalyst and an aqueous H_3PO_4 solution. The experiments were performed in an autoclave. Based on their own results and previous work (Zhao et al., 2009) the authors propose a reaction pathway for cyclohexane formation from phenol which is shown in Figure 3. In Figure 3, the

first, second, and last steps are catalyzed by Pd/C while the third step is catalyzed by the acid that is present. The third step was found to have the lowest turnover frequency (TOF) and the highest activation energy which led them to conclude that the third step was most critical to the reaction. It was found that both the temperature and the amount of acid in the aqueous solution influenced the reaction. At a temperature of 473 K, the reaction of phenol stops at cyclohexanol without the presence of an acid in aqueous conditions. When using the Pd/C catalyst with H_3PO_4, no cyclohexane was formed at 423 K. Increasing the temperature to 473 K and above resulted in cyclohexane becoming the main product. The effects of the metal catalyst were also briefly assessed by using Pd/C, Rh/C, Ru/C and Pt/C catalysts in the conversion of phenol at 473 K with aqueous H_3PO_4, in neutral water and in a basic water solution. The activities of the catalysts were similar in all three different aqueous conditions which led to the authors focusing on the Pd/C catalyst.

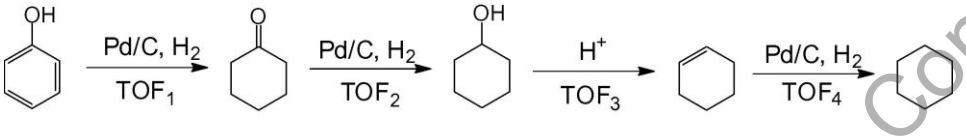

Figure 3. A proposed reaction pathway of cyclohexane formation from phenol using a Pd/C catalyst and an aqueous H_3PO_4 solution at 473 K and 5 MPa H_2. (Zhao et al., 2011; Zhao et al., 2009)

Zhao et al. (2011) proposed a reaction pathway for the HDO of anisole which is shown in Figure 4. The primary reaction steps were found to be the hydrolysis of anisole to phenol and the hydrogenation of phenol to cyclohexanone.

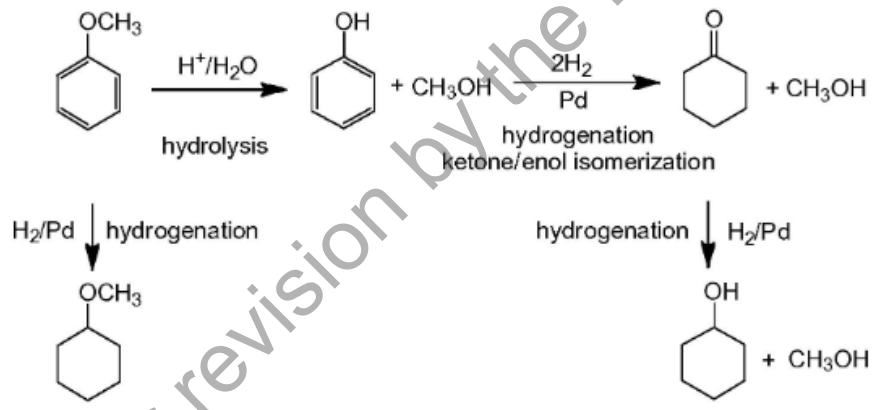

Figure 4. A proposed reaction pathway for anisole using a Pd/C catalyst and an aqueous H_3PO_4 solution at 423 K and 5 MPa H_2. (Zhao et al., 2011)

A proposed reaction pathway for catechol HDO by Zhao et al. (2011) is shown in Figure 5. In the figure two pathways are shown for the formation of cyclohexanone. The primary path was determined to be the one involving ketone hydrogenation and alcohol dehydration.

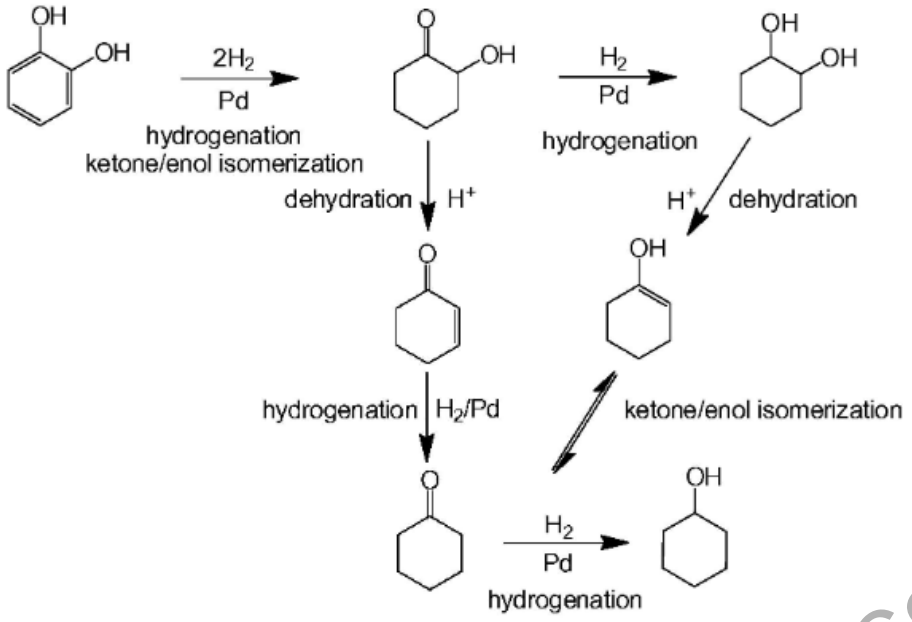

Figure 5. A proposed reaction pathway for catechol using a Pd/C catalyst and an aqueous H_3PO_4 solution at 423 K and 5 MPa H_2. (Zhao et al., 2011)

Zhao et al. (2011) also proposed a reaction network for guaiacol HDO which is shown in Figure 6. The primary reaction pathway for cyclohexanone from guaiacol that is illustrated in Figure 6 is the sequence of hydrogenation of 2-methoxycyclohexanone to methoxycyclohexanol, hydrolysis of methoxycyclohexanol to 1,2-cyclohexanediol, and lastly the dehydration and ketone/enol isomerisation of 1,2-cyclohexanediol.

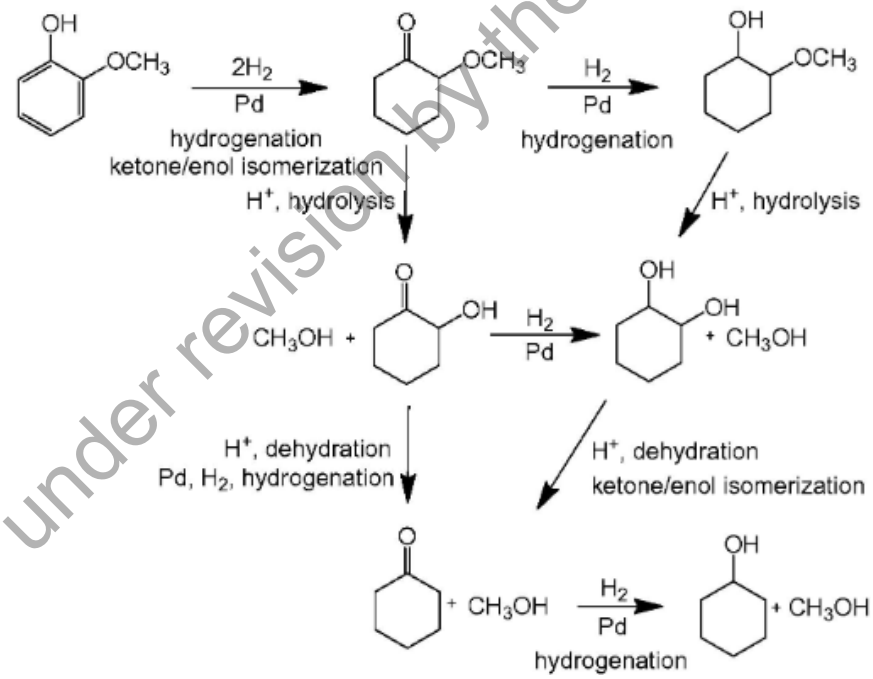

Figure 6. A proposed reaction pathway for guaiacol using a Pd/C catalyst and an aqueous H_3PO_4 solution at 423 K and 5 MPa H_2. (Zhao et al., 2011)

Based on previous research (Zhao et al., 2009) and by combining the reaction pathways of phenol, anisole, catechol and guaiacol, Zhao et al. (2011) present an overall reaction pathway for cycloalkane formation from phenols shown in Figure 7. As can be seen in Figure 3 - Figure 7, the steps are either metal- or acid-catalyzed. The metal component is responsible for the hydrogenation steps and the acid for hydrolysis, dehydration and isomerization. The slowest steps were determined to be the acid-catalyzed dehydration steps.

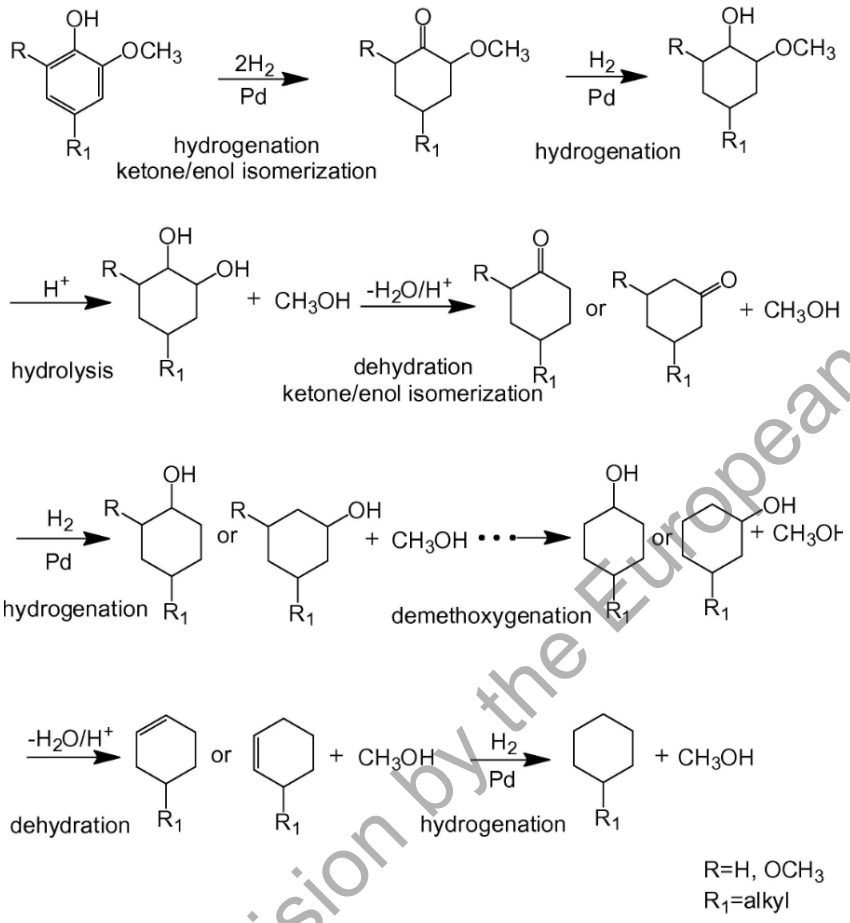

Figure 7. A proposed reaction pathway for the formation of cycloalkanes using a Pd/C catalyst and an aqueous H_3PO_4 solution. (Zhao et al., 2011; Zhao et al., 2009)

Zhao et al. (2011) also studied the effects of the acid in more detail. When using phenol as the reagent, it was found that without the acid, no cyclohexane was formed and most of the product was cyclohexanol. Adding the acid generally increased the selectivity of cyclohexane while significantly decreasing the selectivity of cyclohexanol.

Yu et al. (Yu, Wang, Sun, et al., 2018) studied the aqueous phase hydrodeoxygenation reaction of phenols (phenol, catechol, and o-cresol) over a Ni_3P catalyst. The authors also note that metal phosphides appear to be bi-functional, referring to an older study by Infantes-Molina et al. (2015) (Infantes-Molina et al., 2015). The experiments were done at a temperature of 423 – 623 K and pressure of 4 MPa. A stainless-steel tubular reactor was used. Their results indicated that using a Ni_3P catalyst in the HDO process led to the formation of cycloalkanes instead of

benzenes, agreeing with the reaction networks proposed by Zhao et al. (2009, 2011) shown in Figure 3. Additionally, a similar temperature dependence as the one noted by Zhao et al. (2011) was also observed. At temperatures below 523 K, there was almost no formation of cycloalkanes, whereas the amount of cycloalkanes in the products increased significantly when the temperature was raised above 523 K.

Yu et al. (Yu, Wang, Liu, et al., 2018) further studied the kinetics of the aqueous phase HDO reaction over Ni_3P and Ni_3P-$CePO_4$ catalysts at 523 – 623 K and 4 MPa. The experiments were done in a stainless-steel tubular reactor. The catalyst Ni_3P-$CePO_4$ was analyzed to be even more acidic than the Ni_3P catalyst. The products again mostly consisted of cycloalkanes and no benzenes were detected, suggesting that the reaction followed the pathway proposed by Zhao et al. (2011) shown in Figure 3. Based on their results and as a basis for the kinetic studies, Yu et al. (Yu, Wang, Liu, et al., 2018) propose the following reaction network for phenol which is shown in Figure 8. It was found that the hydrogenation steps of cyclohexanone and cyclohexane were very fast, thus allowing the four steps to be simplified into two effective steps.

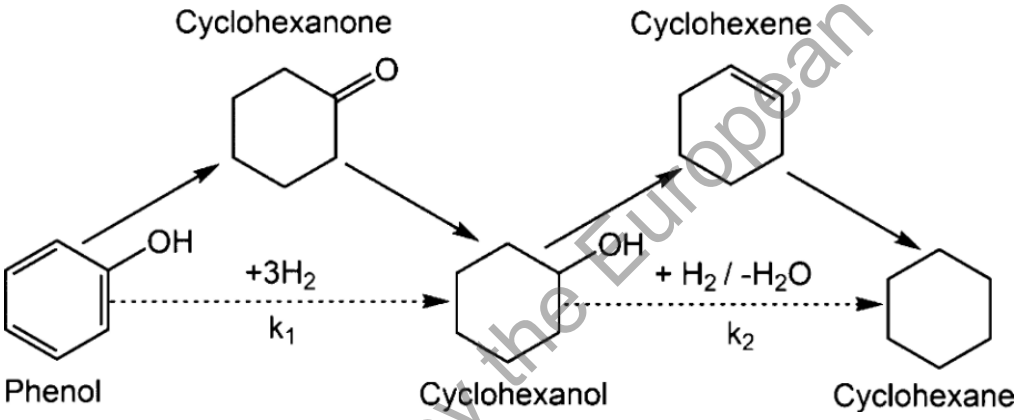

Figure 8. The reaction pathway of phenol in the aqueous phase HDO process using Ni_3P and Ni_3P-$CePO_4$ catalysts. The dashed arrows represent the effective steps of the pathway while the solid arrows represent all the actual steps involved in the pathway. (Yu, Wang, Liu, et al., 2018)

For the determination of the reaction rate constants k_1 and k_2, the conversions of phenol and weight time were used. Weight time is defined in Equation 1 (Yu, Wang, Liu, et al., 2018).

Equation 1.

$$\tau = \frac{w_{cat}}{n_{feed}}$$

, where w_{cat} is the mass of the catalyst (g) and n_{feed} is the total mole flow rate of the feed $\left(\frac{mol}{min}\right)$. In addition to this, the HDO reaction was assumed to be pseudo-first-order in respect to the concentration of phenol and a plug flow reactor described by the following Equation 2 (Yu, Wang, Liu, et al., 2018).

Equation 2.

$$-\ln(1-x) = k\tau$$

, where x is defined as the conversion of phenol and k is the slope. The reaction kinetics were determined over the range of 523 – 623 K and 0,19-0,57 $\frac{g*min}{mol}$. Equation 2 could then be plotted against weight time, showing a clear linear relationship between them. This is shown in Figure 9. The reaction rate constant k_1 could then be evaluated at all the different temperatures by taking the slopes of each line in Figure 9. The same methods were used to evaluate k_2 by using the conversion of cyclohexanol. The values for k_1 were higher than the values for k_2 over the range of 523 - 623 K. (Yu, Wang, Liu, et al., 2018)

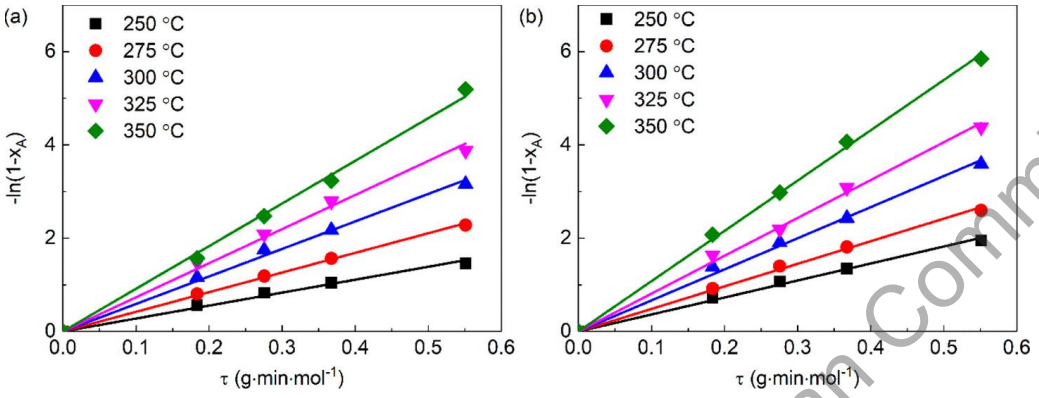

Figure 9. The pseudo-first-order conversion of phenol as a function of weight time. On the left (a) a Ni_3P catalyst is used and on the right (b) a Ni_3P-$CePO_4$. (Yu, Wang, Liu, et al., 2018)

Yu et al. (Yu, Wang, Liu, et al., 2018) also investigated the apparent activation energies by plotting ln k as a function of 1/T as shown in Figure 10. The apparent activation energies were obtained using the slopes of each line in Figure 10 and the Arrhenius equation. The apparent activation energies using Ni_3P were 32 $\frac{kJ}{mol}$ and 123,1 $\frac{kJ}{mol}$ for the first and second effective step respectively. The apparent activation energies using Ni_3P-$CePO_4$ were 28,8 $\frac{kJ}{mol}$ and 103,1 $\frac{kJ}{mol}$ for the first and second effective step respectively. The apparent activation energies for the second effective step were significantly higher than the ones calculated for the first step. The activation energies and the rate constants indicated that the second effective step, where cyclohexanol dehydrates to cyclohexane, was rate determining for the aqueous-HDO of phenol.

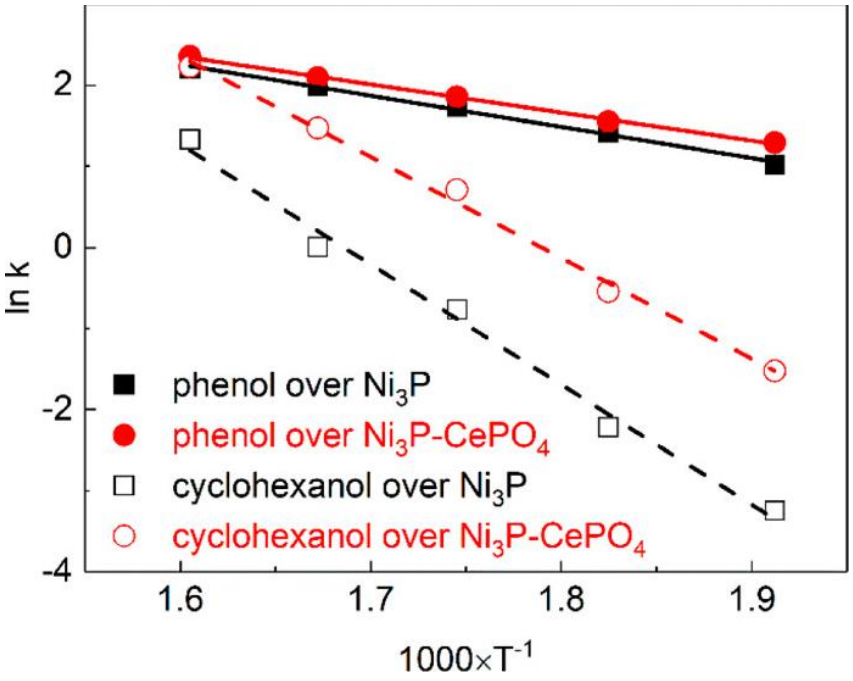

Figure 10. Ln (k) as a function of 1/T for the two effective reaction steps over both Ni_3P and Ni_3P-$CePO_4$ catalysts. (Yu, Wang, Liu, et al., 2018)

As in the previous studies discussed in this report, a temperature dependence was also reported in this study by Yu et al. (Yu, Wang, Liu, et al., 2018), where cyclohexane is not formed when below 523 K. The authors theorize that liquid water suppresses the dehydration of cyclohexanol at temperatures below 523 K, while above 523 K water is a vapor and no longer acts as a suppressant.

Zhang et al. (2016) studied the aqueous-phase HDO of phenols (phenol, anisole, guaiacol and syringol) via simultaneous use of Pd/C catalyst and HZSM-5 zeolite catalyst. The experimental conditions for phenol and anisole were 656 – 746 K and 2 MPa H_2 pressure. The experimental conditions for guaiacol and syringol were 656 – 786 K and 2 MPa H_2 pressure. All experiments were done in a stainless-steel autoclave. The results of the HDO of phenol agreed with previous research, supporting the proposed reaction pathway for phenol, shown in Figure 3, by Zhao et al. (2011, 2009). Experiments using only Pd/C for the HDO of phenol resulted again in the formation of only cyclohexanol, indicating that the acidity of the HZSM-5 catalyst is required for the formation of cyclohexane. Cyclohexane selectivity when concurrently using Pd/C and HZSM-5 was also increased when raising the reaction temperature from 383 K to 443 K. For the conversion of anisole, the authors propose a different reaction pathway shown in Figure 11. The hydrogenation of the aromatic ring is considered the main reaction pathway and there is no hydrolysis pathway as opposed to the one proposed by Zhao et al. (2011) in Figure 4. For anisole also, using either catalyst was not enough for the conversion of cyclohexane and both catalysts had to be used together. The temperature dependence of cyclohexane selectivity was also noticed during the conversion of anisole.

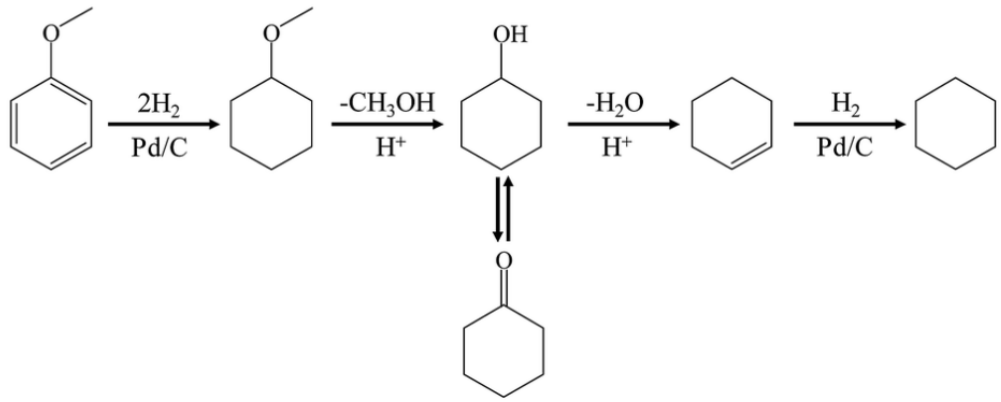

Figure 11. A proposed reaction pathway for anisole using a Pd/C and an HZSM-5 catalyst. (Zhang et al., 2016)

The reaction pathways for guaiacol and 2,6-dimethoxyphenol (syringol) proposed by Zhang et al. (2016) are shown in Figure 12. The pathways for syringol and guaiacol are very similar to the ones proposed by Zhao et al. (2009, 2011) in Figure 6 and Figure 7. There was also temperature dependence present in the conversion of guaiacol and syringol, with the selectivity of single-oxygen-containing compounds increasing with higher temperature.

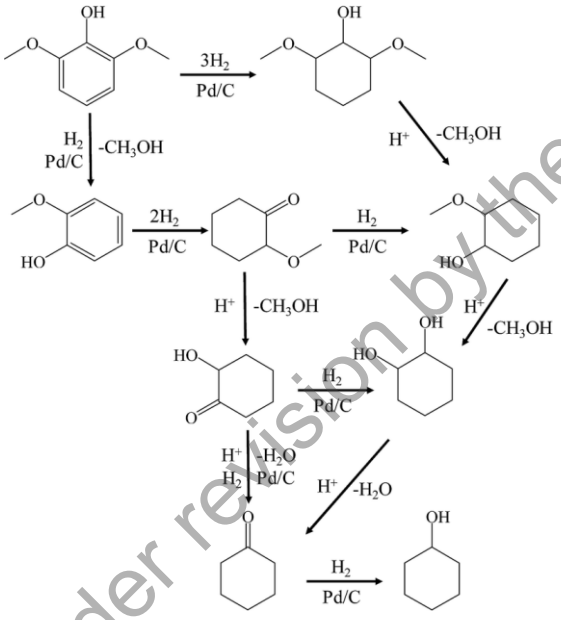

Figure 12. Proposed reaction pathways for guaiacol and 2,6-dimethoxyphenol (syringol) using a Pd/C and an HZSM-5 catalyst. (Zhang et al., 2016)

Another alternative pathway for the aqueous-HDO of anisole also seems to be possible as shown by Saidi et al. (2022) in Figure 13. The experiments took place over the range of 353 – 473 K and 1 – 5 MPa. A batch reactor was used for the experiments. In the pathway in Figure 13 benzene is first formed from anisole which is then hydrogenated to cyclohexane. The hydrogenation of the benzene ring takes place at a different point in the reaction pathway compared to Figure 4, Figure 3 and Figure 11; where there is no benzene observed at all. There was some temperature dependence of benzene and cyclohexane selectivities, with the

temperature dependence itself affected by varying the ratios between nickel and molybdenum in the catalyst. At higher Mo loadings increasing the temperature increased the selectivities of benzene and cyclohexane.

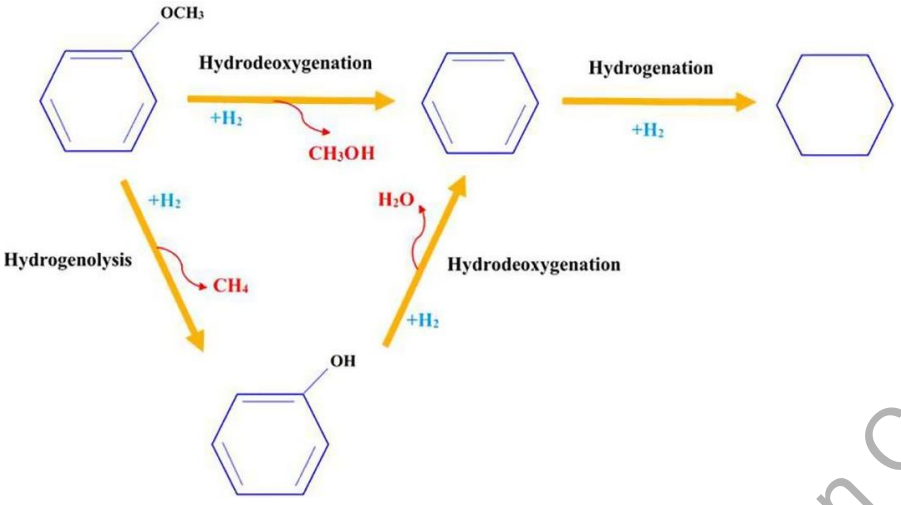

Figure 13. A proposed reaction pathway for anisole using a Ni-Mo NPs@IP catalyst (Saidi & Safaripour, 2022).

Yang et al. (2014) studied the aqueous-phase HDO of phloroglucinol, resorcinol and phenol over a Pt/C catalyst. The experiments were done in a Parr benchtop batch reactor. Based on the main products of the HDO reaction for each reactant, a reaction network was formed for the phenolic compounds, which is shown in Figure 14.

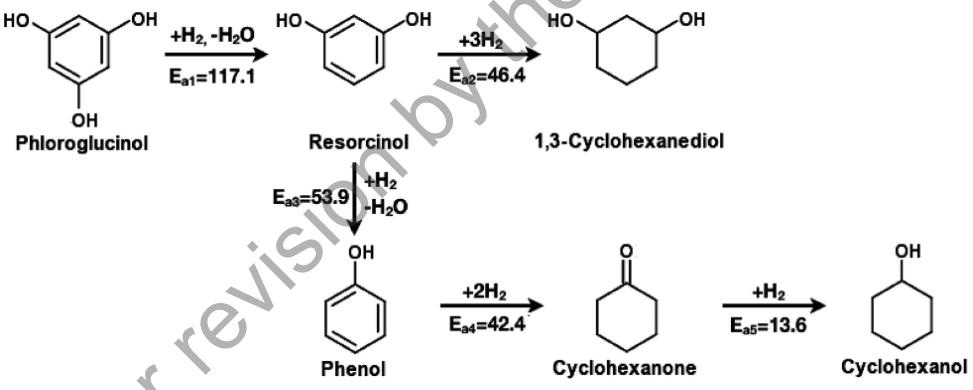

Figure 14. A proposed reaction network for phloroglucinol over a Pt/C catalyst with the experimentally determined activation energies for each step shown as $\frac{kJ}{mol}$. (Yang et al., 2014)

For the evaluation of the rate constants and activation energies of each step in Figure 14, Yang et al. (2014) used first-order kinetics and assumed that adsorption and desorption were at an equilibrium. The reaction rate coefficients were calculated by using non-linear least squares regression on the concentration data. The calculated activation energy of the hydrogenation of phloroglucinol was $117{,}1 \pm 12{,}9\ \frac{kJ}{mol}$. For the hydrogenation of resorcinol, the activation energy was $46{,}4 \pm 4{,}7\ \frac{kJ}{mol}$ in the formation of 1,3-cyclohexanediol and $53{,}9 \pm 1{,}7\ \frac{kJ}{mol}$ in the

formation of phenol. Lastly the hydrogenation of phenol and cyclohexanone had activation energies of $42{,}4 \pm 4{,}2\ \frac{kJ}{mol}$ and $13{,}6 \pm 1{,}2\ \frac{kJ}{mol}$ respectively. The kinetic equations derived by the authors won't be shown here as they seemed unconventional.

2.1.3 Hydrothermal HDO of benzofuran

The kinetics of hydrothermal HDO of benzofuran was studied by Dickinson et al. (2012). The experiments were done in supercritical water at 653 K using a 5 wt.% Pt/C catalyst in a batch reactor. The reaction network for benzofuran was studied by first using benzofuran as a reagent and then using the resulting major products (ethylphenol, ethylbenzene, ethylcyclohexanone, ethylcyclohexanol and ethylcyclohexane) as reagents. The loading ratio of hydrogen to the reagents was also varied. The experiments were thus grouped by the reactant and the hydrogen ratio. The water loading was found to affect the product distribution, with an increased amount of water resulting in less deoxygenated and hydrogenated products. The authors speculate the cause to be water binding to the surface of the metal, leaving less sites for the reactants. Analyzing the products of each component, the authors proposed the following reaction pathways from benzofuran which is shown in Figure 15. It shows the different steps for which the authors evaluated the reaction rate constants.

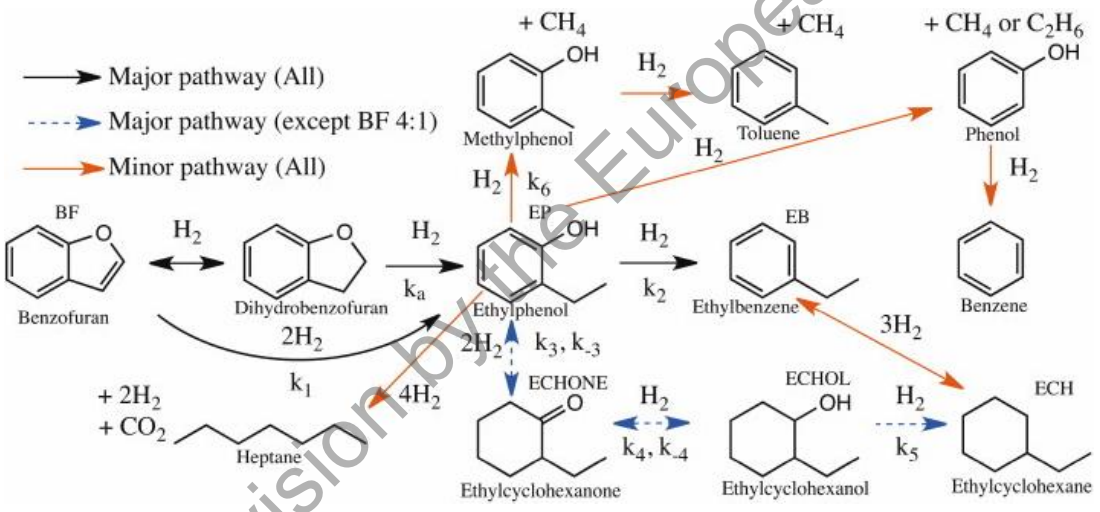

Figure 15. Proposed reaction pathway for benzofuran in hydrothermal HDO using supercritical water. (Dickinson et al., 2012)

Figure 15The kinetic model that Dickinson et al. (2012) derived are shown in Equation 3 - Equation 9.

Equation 3

$$\frac{1}{w}\frac{dC_{BF}}{dt} = -k_1 C_{BF} C_{H_2}$$

Equation 4

$$\frac{1}{w}\frac{dC_{EP}}{DT} = k_1 C_{EP} C_{H_2} - \frac{C_{EP} C_{H_2}(k_2 + k_6)}{1 + K_1 C_{BF}} - k_3 C_{EP} C_{H_2}^2 + k_{-3} C_{ECHONE}$$

Equation 5

$$\frac{1}{w}\frac{dC_{EB}}{dt} = \frac{k_2 C_{EP} C_{H_2}}{1 + K_1 C_{BF}}$$

Equation 6

$$\frac{1}{w}\frac{dC_{ECHONE}}{dt} = k_3 C_{EP} C_{H_2}^2 - k_{-3} C_{ECHONE} - k_4 C_{ECHONE} C_{H_2} + k_{-4} C_{ECHOL}$$

Equation 7

$$\frac{1}{w}\frac{dC_{ECHOL}}{dt} = k_4 C_{ECHONE} C_{H_2} - k_{-4} C_{ECHOL} - k_5 C_{ECHOL} C_{H_2}$$

Equation 8

$$\frac{1}{w}\frac{dC_{ECH}}{dt} = k_5 C_{ECHOL} C_{H_2}$$

Equation 9

$$\frac{1}{w}\frac{dC_{H_2}}{dt} = -2k_1 C_{BF} C_{H_2} - \frac{C_{EP} C_{H_2}(k_2 + k_6)}{1 + K_1 C_{BF}} - 2k_3 C_{EP} C_{H_2}^2 + 2k_{-3} C_{ECHONE} - k_4 C_{ECHONE} C_{H_2} + k_{-4} C_{ECHOL} - k_5 C_{ECHOL} C_{H_2}$$

, where w is the catalyst mass (g). It should be noted that Equation 3 - Equation 9 have all been written as they were presented in the corrigendum of the study by Dickinson et al. (2012). There seems to be a mistake in Equation 4 with the term "$k_1 C_{EP} C_{H_2}$" and it should instead be written as "$k_1 C_{BF} C_{H_2}$" since step 1 is shown to be irreversible in Figure 15. The differential equations were derived by combining the design equation for batch reactors with the rate equations of each major reaction path. Dickinson et al. (2012) state that the reaction orders for each reaction are according to its stoichiometry except for the first reaction of benzofuran. The amount of dihydrobenzofuran in the reaction products was very small, which led the authors to assume that the hydrogenolysis of dihydrobenzofuran to ethylphenol happened instantaneously. Thus, the rate constant k_1 could be assumed to apply to the hydrogenation of benzofuran and hydrogenolysis of dihydrobenzofuran. The experimental results indicated that benzofuran inhibited reaction 2 (direct deoxygenation of ethylphenol to ethylbenzene) and the minor reaction 6 (ethylphenol to form methylphenol) in Figure 15. This inhibition is present in reactions 2 and 6 as the term "$1 + K_{BF} C_{BF}$" in the denominators of the rate equations. The values of the rate constants were then optimized, and the optimized values indicated that in the presence of benzofuran, reaction 2 was the rate-limiting step.

For the evaluation of the kinetic model, Dickinson et al. (2012) compared the calculated and experimentally achieved concentrations for each component and plotted these as a function of time. The errors between the experimental values and the calculated values were also calculated for each experimental dataset to determine possible favoritism towards a particular dataset. Validation of the model was done by using a slightly different data set than the ones used to optimize the kinetic model. The calculated and experimental concentrations were again compared to determine the validity of the model.

2.2 Non-hydrothermal HDO

In this chapter studies on the kinetics of non-hydrothermal HDO will be presented and compared against the ones presented in Chapter 2.1 to discover the possible effects that an aqueous or hydrothermal environment might have on the kinetics of HDO. Because of this, the studies discussed in this chapter are mostly restricted to the ones that use similar catalysts as in chapter 2.1. Additionally, studies using sulphided NiMo or Ru/C and similar catalysts will be discussed more specifically as the experiments done at VTT in the BL2F project utilized these two catalysts.

2.2.1 Non-hydrothermal HDO of real oils

Oh et al. (2015) studied the kinetics of non-hydrothermal HDO of bio-oils. The bio-oil was produced from Miscanthus Sinensis using fast pyrolysis. Supercritical ethanol was used as a solvent. The effect of catalysts was determined using Ru/C and Pt/C catalysts. The temperature range for the experiments was 523 – 623 K. An autoclave was used for the experiments. The proposed reaction network for low molecular weight products by the authors is shown in Figure 16.

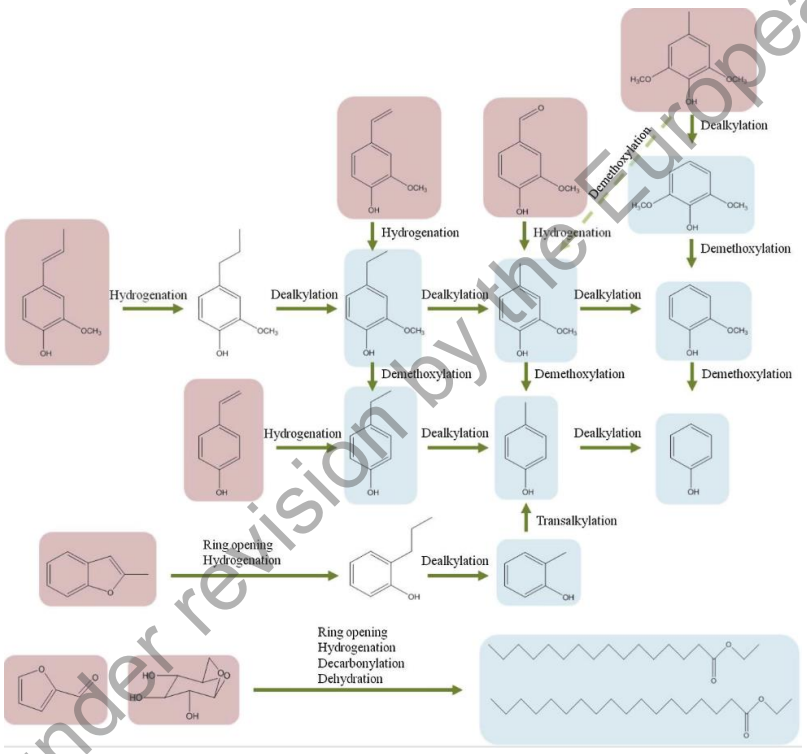

Figure 16. A proposed reaction network for the low molecular weight compounds in the HDO of bio-oil using Ru/C and Pt/C catalysts at 523 – 623 K. The reactants in the bio-oil are colored in red, the products in the heavy oil phase are colored in blue and those without color are the assumed intermediates by the authors. (Oh et al., 2015)

2.2.2 Non-hydrothermal HDO of phenols

Yang et al. (2021) studied the kinetics of HDO using a combination of H_2WO_4 and Ru/C as catalysts. Octane was used as a solvent. Both a mixture and pure phenolic model compounds

were used as reactants in this experiment. The mixture of compounds was acquired by the pyrolysis of cotton straw followed by the separation of the phenolic compounds using fractional condensation. The final reaction temperature of 533 K was achieved by a heating rate of around 6 K/min. The experiments were done in a stainless-steel autoclave. The authors propose a reaction network for guaiacol which is shown in Figure 17. Compared to Figure 6 and Figure 12, Figure 17 shows a slightly different reaction path that includes the formation of phenol.

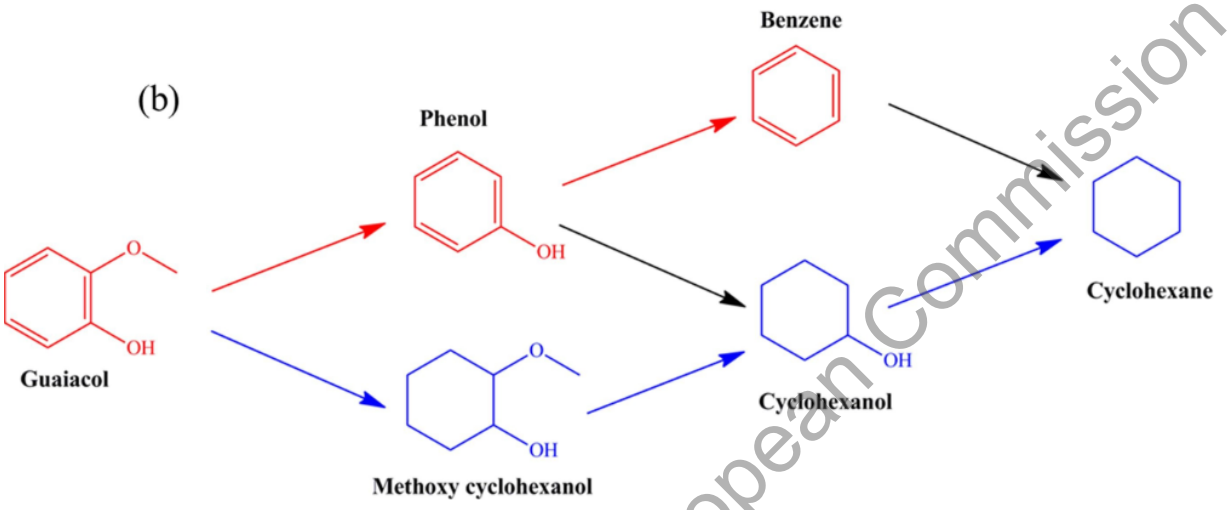

Figure 17. Guaiacol reaction network using Ru/C and H_2WO_4 at 533 K. Two pathways are present in blue and red. The blue pathway is the primary path at sufficient hydrogen pressures while they are both primary when the process is operated with insufficient hydrogen pressure. (Yang et al., 2021)

Yang et al. (2021) also studied the effects that hydrogen pressure has on the HDO process. At low hydrogen pressures below 0,5 MPa, the reaction happens through both pathways presented in Figure 17. At sufficiently high hydrogen pressures, determined to be 1 MPa in the experiment by Yang et al. (2021), the blue pathway shown in Figure 17 becomes the primary path. The authors also noted the same temperature dependence that was discussed in chapter 2.1, where the reaction seemed to stop at cyclic alcohols at insufficient temperatures, with the selectivity of cyclohexane increasing with the reaction temperature, reaching nearly 100 % at 553 K.

In addition to aqueous-phase HDO, Yu et al. (Yu, Wang, Sun, et al., 2018) also studied the HDO of phenolic compounds in oil-phase solvent (decalin). The results of the HDO of phenol and o-cresol indicated that their reactions proceeded according to a similar route as their aqueous-phase counterparts. Additionally, the oil-phase reactions using Ni_3P also produced significantly more cycloalkanes at temperatures of 523 K and lower.

Şenol et al. (2007) studied the HDO of phenol over sulphided NiMo/γ-Al_2O_3 and CoMo/γ-Al_2O_3 catalysts. A batch reactor was used for the experiments in liquid-phase and a flow reactor for the experiments in gas-phase. The gas-phase experiments were done at 523 K and 1,5 MPa. The liquid-phase experiments were done at 523 K and 7,5 MPa hydrogen pressure. All experiments used hydrogen gas. In addition to the reactants, the environment also contained

a mixture of H_2S/H_2. To determine the reaction networks, the authors also used cyclohexanol and cyclohexanone as reactants, as they were products in the HDO of phenol. The reactions of benzene were also studied. Based on the results of these experiments, a reaction network was formed which is shown in Figure 18.

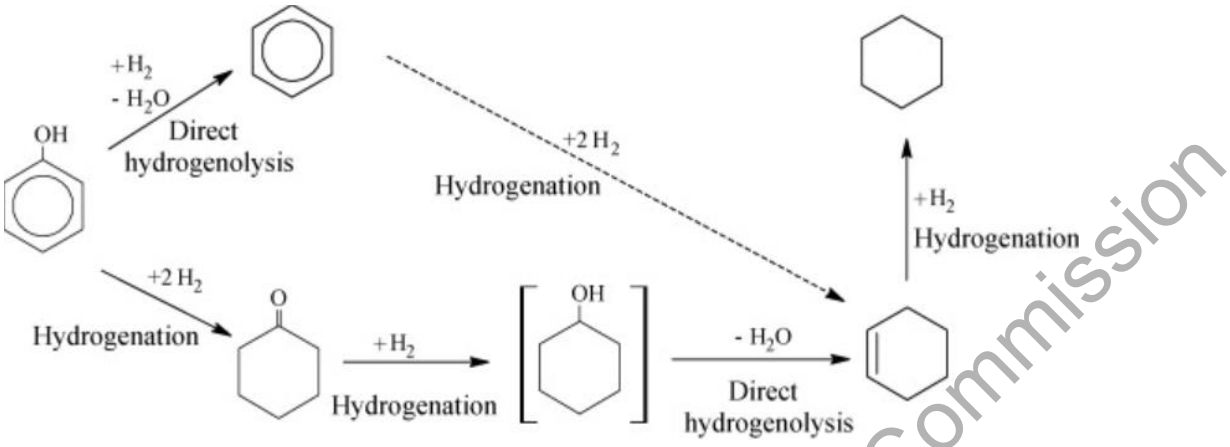

Figure 18. A proposed reaction network for phenol in HDO using sulphided NiMo/γ-Al_2O_3 and CoMo/γ-Al_2O_3 catalysts. The dashed line indicates a reaction deemed insignificant by the authors. (Şenol et al., 2007)

In addition to Figure 18, Şenol et al. (2007) also proposed another reaction network which is shown in Figure 19 for cyclohexanol in the presence of a sulphiding agent. In Figure 19 cyclohexene is shown to be formed by elimination reactions, while the steps forming cyclohexanethiol are nucleophilic substitution reactions. When comparing Figure 18 with Figure 13 by Saidi et al. (2022), the formation of phenol can happen through a similar route. There are some differences, like the missing of cyclohexene within Figure 13, however the major difference is that Şenol et al. (2007) considered the hydrogenation route of benzene to cyclohexene to be insignificant in the formation of cyclohexane. Indeed, the reaction network presented in Figure 18 is much more like the one proposed by Zhao et al. (2011) shown in Figure 3, despite both studies using different catalysts. Saidi et al. (2022) and Şenol et al. (2007) both used similar catalysts, with key differences in experimental conditions being aqueous-phase HDO by Saidi et al. (2022) and the use of sulphiding agents by Şenol et al. (2007). Despite Şenol et al. (2007) arguably having more differences in the experimental conditions with Zhao et al. (2011) than with Saidi et al. (2022), the proposed reaction networks are more similar. This may also indicate that the Ni-Mo NPs@IP catalyst used by Saidi et al. (2022) is significantly different from the NiMo/γ-Al_2O_3 catalyst used by Şenol et al. (2007), despite having similar active substances. This makes evaluating the contribution of the aqueous-phase to the kinetics of HDO more complicated and the differences in the kinetics may be due to multiple different factors as opposed to a singular one.

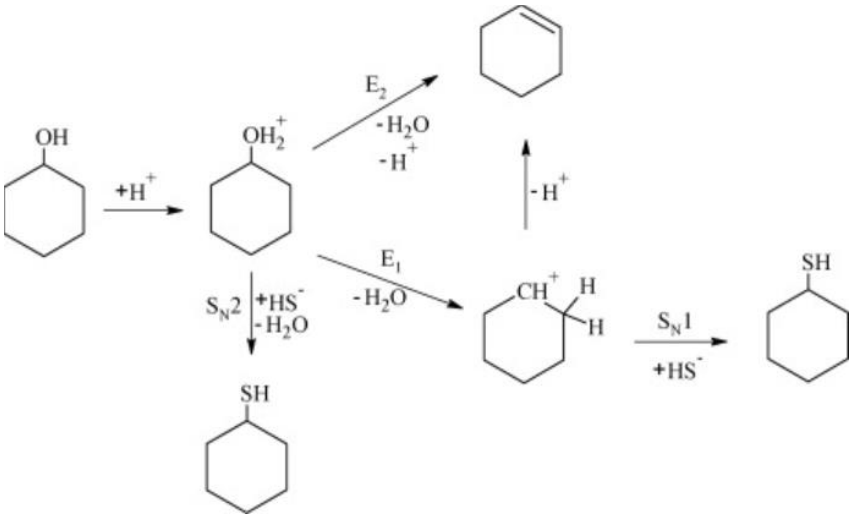

Figure 19. Cyclohexanol reaction network to cyclohexene and cyclohexanethiol in the presence of sulphiding agents. (Şenol et al., 2007)

Romero et al. (2010) studied the HDO kinetics of 2-ethylphenol on sulphided Mo/Al_2O_3-based catalysts that were NiMo/γ-Al_2O_3 and CoMo/γ-Al_2O_3. They used a high-pressure fixed-bed microreactor with the conditions of 613 K and 7 MPa total pressure. The reactant 2-ethylphenol was diluted with toluene. The authors proposed a reaction network for 2-ethylphenol which is shown in Figure 20. The Figure shows 3 different initial steps for 2-ethylphenol to react to. These were the hydrogenation path (HYD), the direct deoxygenation path (DDO), and the acid-catalyzed path (ACI) that happens through interactions with the catalyst support (γ-Al_2O_3). The hydrogenation pathway begins with the hydrogenation of the aromatic ring, forming 2-ethylcyclohexanol. The authors however were unable to detect this compound, which was theorized to be due to the compound rapidly dehydrating. For the formation of ethylcyclohexene, the authors noted a ratio of about 3:1 for 1-ethylcyclohexene and 3-ethylcyclohexene. In the DDO path, ethylbenzene is formed through C-O-bond splitting. The final path involved only the γ-Al_2O_3 support leading to disproportionation and isomerization reactions. The authors have also studied the mechanisms of the three pathways in more detail, but they will not be discussed here.

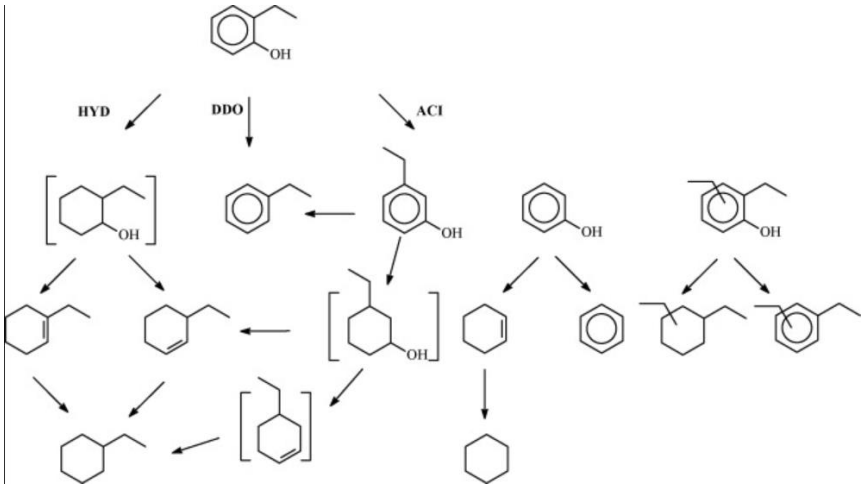

Figure 20. A proposed reaction network for 2-ethylphenol via sulphided Mo-based catalysts. The []-brackets indicate compounds that the authors were unable to detect in the reaction mixture. (Romero et al., 2010)

In Chapter 2.1 there is not much information on the reactions of 2-ethylphenol in aqueous conditions to make comparisons to the study by Romero et al. (2010). The only comparison can be made with the study by Dickinson et al. (2012). Even though they used different catalysts as Romero et al. (2010), the reaction pathways for 2-ethylphenol remain somewhat similar. The final products of ethylbenzene and ethylcyclohexane was the same in both studies. Additionally, both studies somewhat agree on the formation of ethylcyclohexane from ethylbenzene with Romero et al. (2010) proposing that it does not happen, and Dickinson et al. (2012) keeping it a minor reaction. Interestingly, Dickinson et al. (2012) included ethylcyclohexanone into their reaction network, while Romero et al. (2010) did not. Lastly the third route by Romero et al. (2010) was attributed to the catalyst support, which could explain the differences between the ACI route in Figure 20 and the other minor reaction routes in Figure 15 by Dickinson et al. (2012). Based on these two studies, it seems that the differences in the experimental conditions didn't have significant effects on the reaction networks of the HDO reaction of 2-ethylphenol. The reaction network for phenol in Figure 18 by Şenol et al. (2007) was also very similar to the one shown in Figure 20.

Nimmanwudipong et al. (2011) studied the kinetics of HDO using guaiacol as a model compound via Pt/γ-Al_2O_3 and HY zeolite catalysts. The experiments used a continuous tubular reactor at a temperature range of 523 – 623 K. The authors proposed a reaction network for the primary products in guaiacol HDO which is shown in Figure 21, which was based on the observed product distribution and selectivities. The rate constant for catechol formation was calculated from the overall yield of catechol in units of $\frac{l}{g\ (catalyst)*h}$. The rate constant for the hydrogenolysis of catechol was then calculated by substracting the rate constants of the other catechol reactions from the overall rate constant for catechol formation.

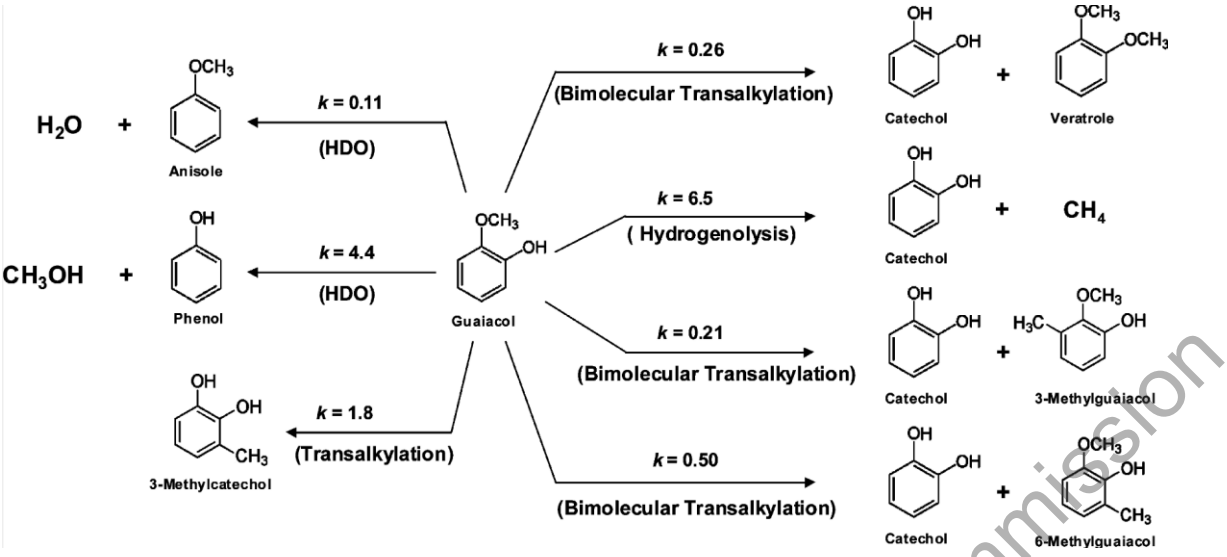

Figure 21. A proposed reaction network for the primary products of guaiacol HDO via Pt/ γ-Al_2O_3 at 573 K. The values of k shown are pseudo-first-order rate constants with units of $\frac{l}{g\,(catalyst)*h}$. (Nimmanwudipong et al., 2011)

Nimmanwudipong et al. (2011) also proposed an extended qualitative reaction network of the one shown in Figure 21. The extended reaction network is presented in Figure 22.

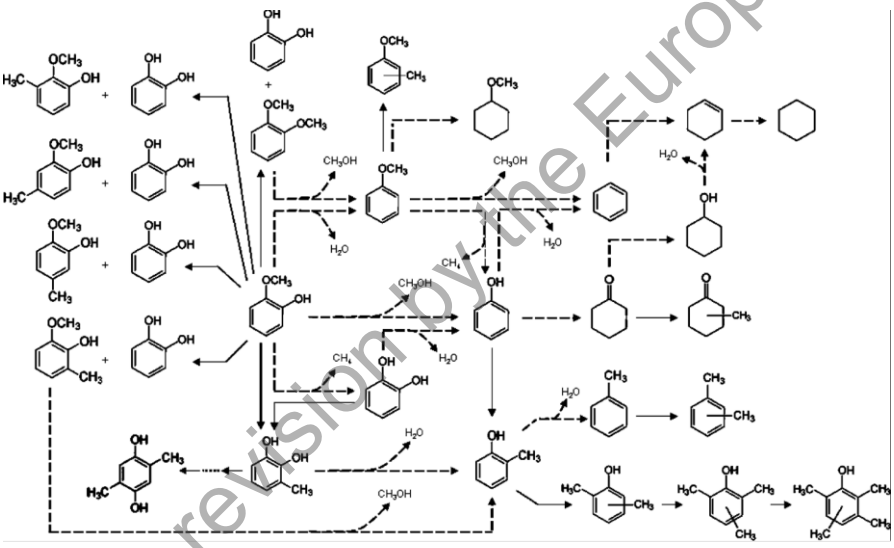

Figure 22. An extended reaction network for the products of guaiacol HDO via Pt/ γ-Al_2O_3 at 573 K. The dashed arrows represent HDO, hydrogenolysis and hydrogenation reactions while the solid arrows represent methyl group transfer reactions. (Nimmanwudipong et al., 2011)

Nimmanwudipong et al. (2011) also noted a temperature dependence in the HDO reaction for the selectivities of the products. Compared to the earlier studies discussed in chapter 2.1 however, the dependency was not as uniform. The selectivities of the HDO reactions and veratrole formation decreased with increasing temperature, the selectivities of the transalkylation reactions increased with increasing temperature, and the selectivity of catechol

formation first increased when temperature was raised to 573 K and then decreased when temperature was 623 K.

Comparing Figure 22 by Nimmanwudipong et al. (2011) to the reaction networks of guaiacol HDO shown in chapter 2.1, (Figure 6 and Figure 12) there are significant differences. In the reaction network proposed by Nimmanwudipong et al. (2011), most of the products are aromatic and lose their aromaticity during the last few steps of the reaction. Zhao et al. (2011) and Zhang et al. (2016) both similarly propose that the hydrogenation of the aromatic ring happens immediately before any other step. The largest difference here is the use of Pt in the catalyst instead of Pd and the hydrothermal/aqueous conditions and the differences in the reaction networks could be due to these factors. Comparing to non-hydrothermal/aqueous HDO studies, in Figure 17, proposed by Yang et al. (2021), that was discussed earlier in this chapter, there is a route for guaiacol HDO where the aromatic ring is hydrogenated during the last step of the overall reaction. This route was stated to occur at low hydrogen pressures. The highest system pressure that Nimmanwudipong et al. (2011) used was 0,14 MPa, which is significantly less than the 0,5 MPa lower bound where Yang et al. (2021) described this route to occur. Nimmanwudipong et al. (2011) also noted oxygen removal increasing with higher hydrogen partial pressures. As Zhao et al. (2011) and Zhang et al. (2016) used 5 MPa and 2 MPa hydrogen pressures respectively, it is likely that the differences between the reaction networks for guaiacol in said studies and the one in Nimmanwudipong et al. (2011) is due to the large difference in hydrogen pressure. Nonetheless, the reaction networks by Nimmanwudipong et al. (2011) might be an accurate representation of the reactions of guaiacol in low H_2 pressure HDO.

Lin et al. (2011) studied the HDO of guaiacol over Rh-based and sulphided Mo-based catalysts. The Rh-based catalysts were Rh/ZrO_2, $PtRh/ZrO_2$ and $PdRh/ZrO_2$. The Mo-based catalysts were $CoMo/Al_2O_3$ and $NiMo/Al_2O_3$. A batch reactor was used with a tetradecane ($C_{14}H_{30}$) solvent. Experiments were conducted at 573 – 673 K and 5 MPa hydrogen pressure. The authors proposed two reaction networks for the HDO of guaiacol for the types of catalysts used in the study. The reaction networks are shown in Figure 23 and Figure 24. The two reaction networks differ mainly by the sequence of the steps. The first step on the Rh-based catalysts is the hydrogenation of the aromatic ring, while on the CoMo and NiMo catalysts the first step is demethylation, demethoxylation or deoxygenation.

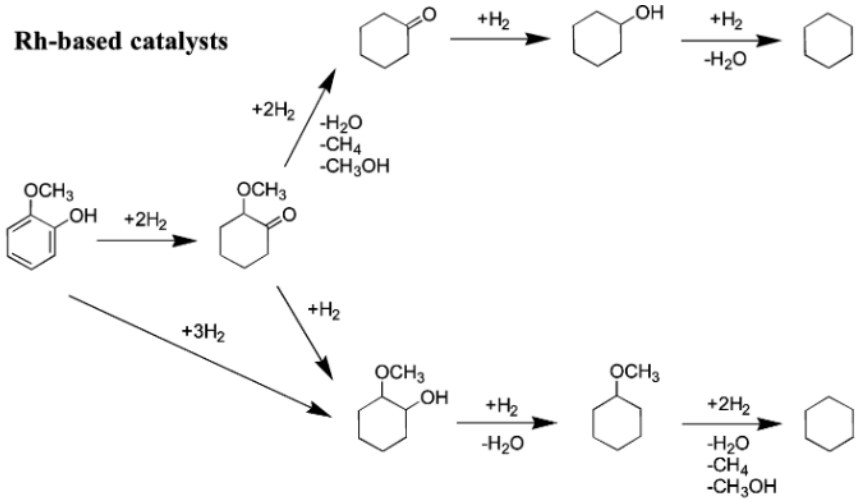

Figure 23. A proposed guaiacol reaction network in HDO via Rh-based catalysts. (Lin et al., 2011)

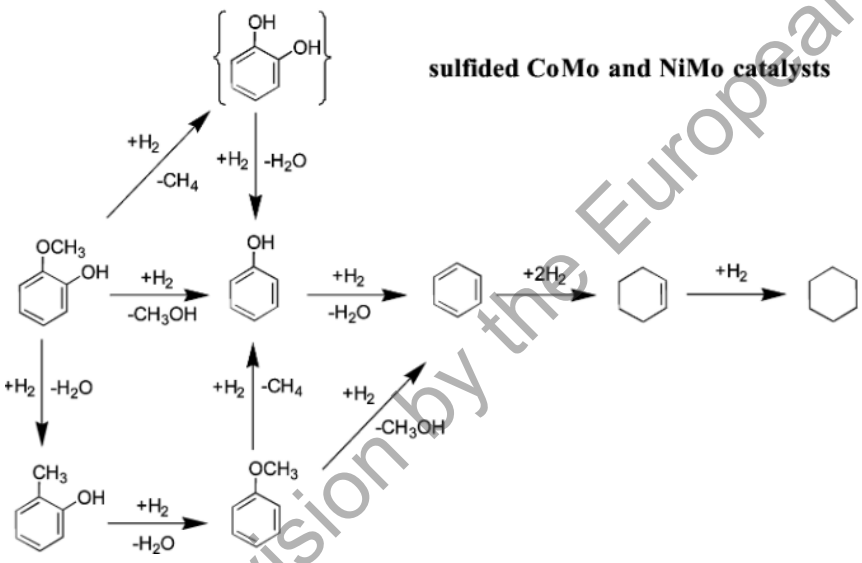

Figure 24. A proposed guaiacol reaction network in HDO via sulphided CoMo and NiMo catalysts. (Lin et al., 2011)

Lin et al. (2011) also noted a temperature dependence with the yield of cyclohexane increasing with temperature when using the Rh-based catalysts. Additionally, on the CoMo and NiMo catalysts, no other products besides coke formed when temperature was under 573 K.

When comparing the reaction network of guaiacol on the Rh-based catalysts shown in Figure 23 with the ones shown in Figure 6 and Figure 12, the overall sequence is similar, with the hydrogenation step happening at the very beginning. There are some differences in the intermediate products like there being no cyclohexanediol in Figure 23. Zhao et al. (2011) did assess that Pd/C and Rh/C catalysts were roughly the same in terms of activity for phenol HDO. These studies indicate that Rh/C and Pd/C are similar enough that they produce similar reaction networks during HDO. Again the temperature is unlikely to be a determining factor in the

differences between the reaction networks, and the same applies to H_2 pressure. In this case, it is also possible that the hydrothermal/aqueous experimental conditions affect the reaction network.

The reaction network of the sulphided NiMo and CoMo catalysts more closely resembles Figure 13, where the hydrogenation happens at the end of the reaction. Even if only for phenol, Figure 18 seems to contradict this observation, with the hydrogenation happening very early on in the reaction or not at all. Since the experiments were done at 5 MPa H_2 pressure, it's unlikely that raising the H_2 pressure any further would modify the reaction network, since it is already well above the 0,5 – 1 MPa range that was given by Yang et al. (2021).

Hellinger et al. (2015) studied the kinetics of guaiacol HDO via Pt-based catalysts with varying supports. A batch reactor was used for the experiments. Guaiacol was fed to the reactor as a solution containing n-hexadecane. The experimental conditions were 303 – 523 K and 0,1 – 9 MPa H_2. The authors generally agreed with the reaction network proposed by Lin et al. (2011) for the Rh-based catalysts shown in Figure 23, which according to Hellinger et al. (2015) seems typically applicable to noble metal catalysts. Hellinger et al. (2015) propose their own altered reaction network based on their results. The reaction network is shown in Figure 25. While the highest experimental temperature in this study was 523 K, the authors state that they have focused on temperatures below 473 K. The difference between Figure 23 and Figure 25 begin at the first step, where methoxycyclohexanone is replaced by methoxycyclohexanol. Otherwise, the reaction network remains the same with the first step followed by hydrogenation of either oxygen containing functional group, with the final product being cyclohexane. Overall, the reaction networks remain structurally almost identical. Although relatively low temperatures were used for HDO in this study, Lin et al. (2011) used higher temperatures and still achieved similar results. This might indicate that temperature has no effect on the general reaction network of guaiacol HDO.

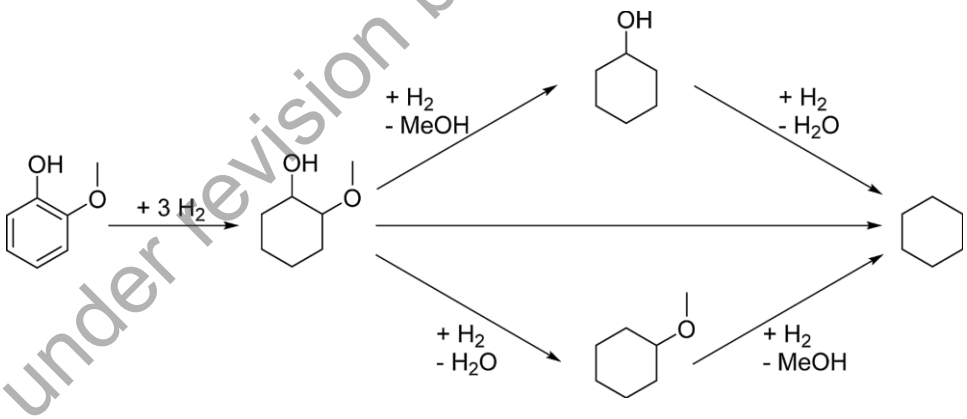

Figure 25. A proposed reaction network for guaiacol HDO via noble metal catalysts below 473 K. (Hellinger et al., 2015)

Another study related to the kinetics of guaiacol HDO on noble metal catalysts was done by Lee et al. (2016). In this study, the authors used bifunctional catalysts Pt/HY and Pt/HZSM-5. A batch reactor was used with decane acting as a solvent for the guaiacol. The experimental conditions were 523 K and 4 MPa H_2 pressure. The authors propose a reaction network for

guaiacol HDO based on their results and previous reports on the subject. The reaction network is shown in Figure 26.

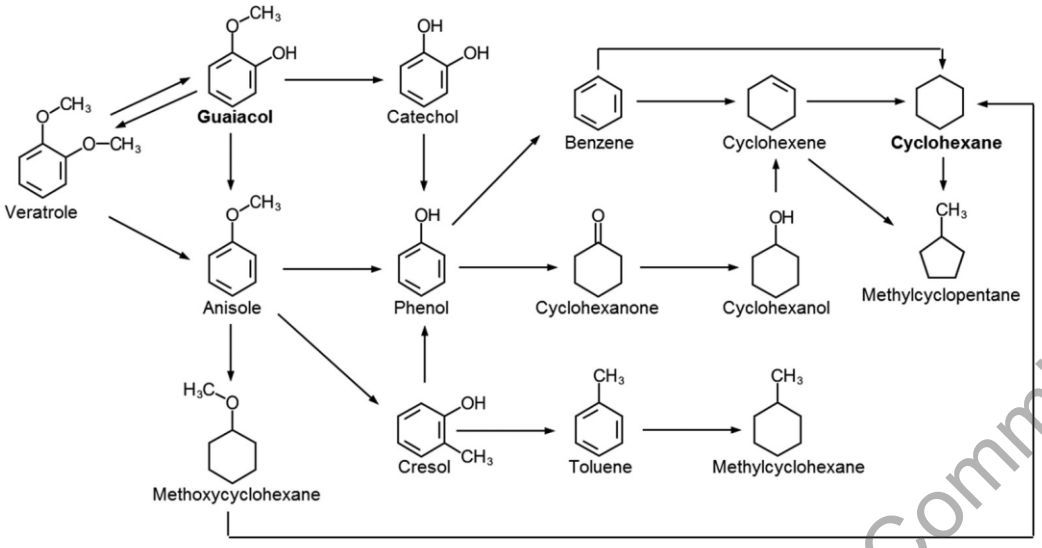

Figure 26. A proposed reaction network for guaiacol HDO via Pt/HY. (Lee et al., 2016)

In addition to guaiacol, the HDO of veratrole, phenol and anisole was also performed. Lee et al. (2016) note that veratrole was formed as a reaction intermediate of guaiacol HDO and vice versa, indicating that the compounds are convertible to one another. The authors also noticed temperature dependencies for the conversion of phenol and anisole. Significant amounts of cyclohexanol were found in the products of phenol HDO at 423 K, while no cyclohexanol was detected in the products at 523 K. Small amounts of 1-methoxycyclohexane was present in the products of anisole HDO at 423 K, while none was detected again at 523 K.

Based on the study by Lee et al. (2016), it seems that the HDO of guaiacol does not begin with the immediate hydrogenation of the aromatic ring, instead having it take place in the middle or at the end of the overall reaction. Compared to the previous studies presented in this deliverable report, Figure 26 most closely resembles the reaction networks proposed by Nimmanwudipong et al. (2011). Similar types of catalysts were used by both Zhao et al. (2011) and Zhang et al. (2016), with comparable experimental conditions also. This could indicate that the differences are caused by the absence of hydrothermal/aqueous experimental conditions. The decane solvent was tested by Lee et al. (2016) to not take part in the HDO reaction, so its effect on the reaction networks should be minimal.

Liu et al. (2017) studied the kinetics of guaiacol HDO on Ru, Pd and Mo_2C catalysts using activated carbon as a support material. The experiments used a batch reactor and decalin as solvent. The experimental conditions were 513 – 603 K for the Pd/AC and Ru/AC catalysts and 603 – 648 K for Mo_2C/AC catalyst. In all three cases 3,4 MPa initial H_2 pressure was used. The authors proposed the following three reaction networks for guaiacol HDO for each catalyst shown in Figure 27, Figure 28 and Figure 29 based on the experimental product distributions as well as other studies found in literature. Additionally, the authors derived kinetic models for each reaction network by grouping similar reactions together and defining reaction rate constants for each group.

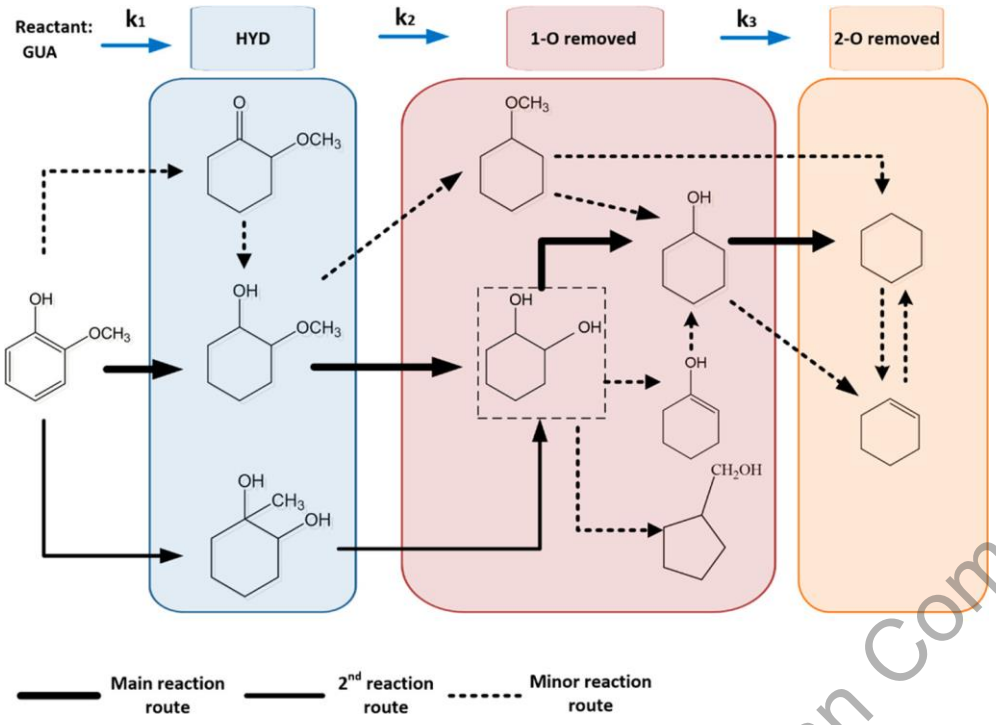

Figure 27. A proposed reaction network for guaiacol HDO via Pd/AC catalyst. Compounds within dotted squares were not detected by the authors but were instead added to the reaction network by the authors based on literature. (Liu et al., 2017)

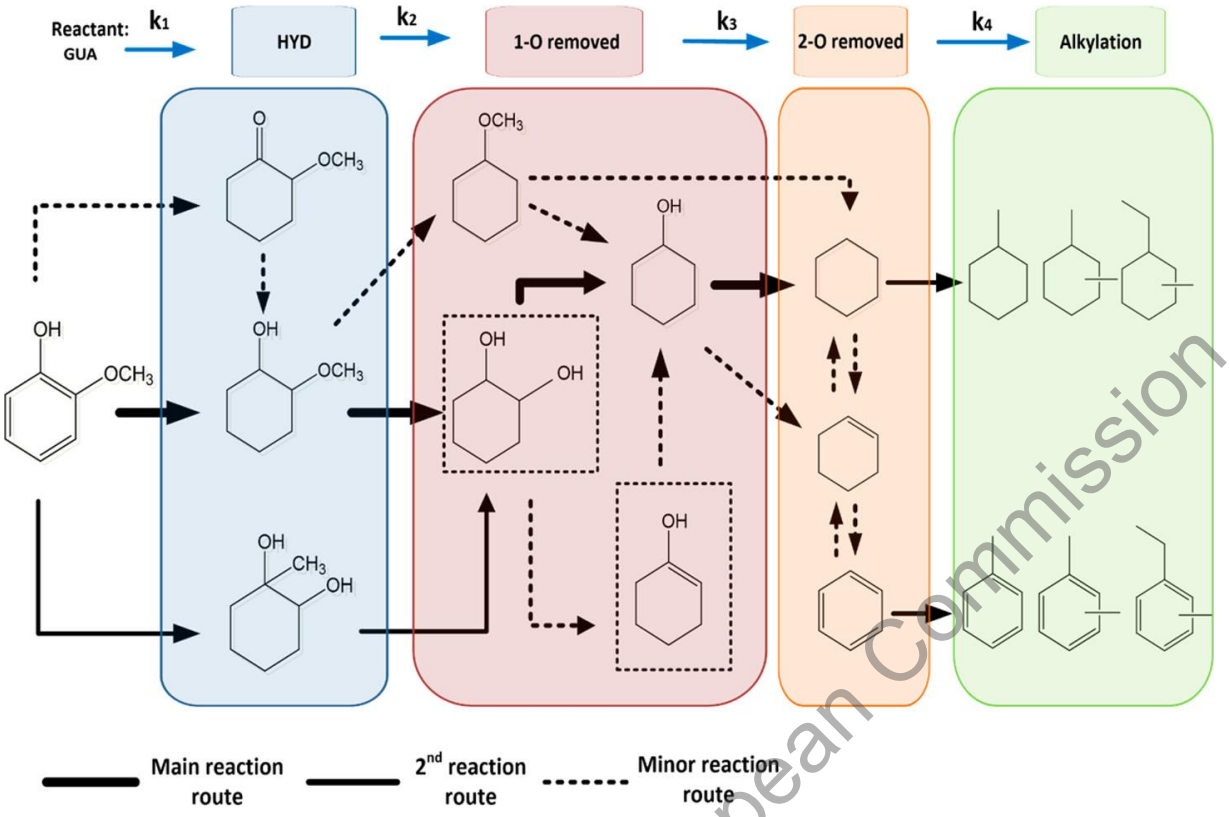

Figure 28. A proposed reaction network for guaiacol HDO via Ru/AC catalyst. Compounds within dotted squares were not detected by the authors but were instead added to the reaction network by the authors based on literature. (Liu et al., 2017)

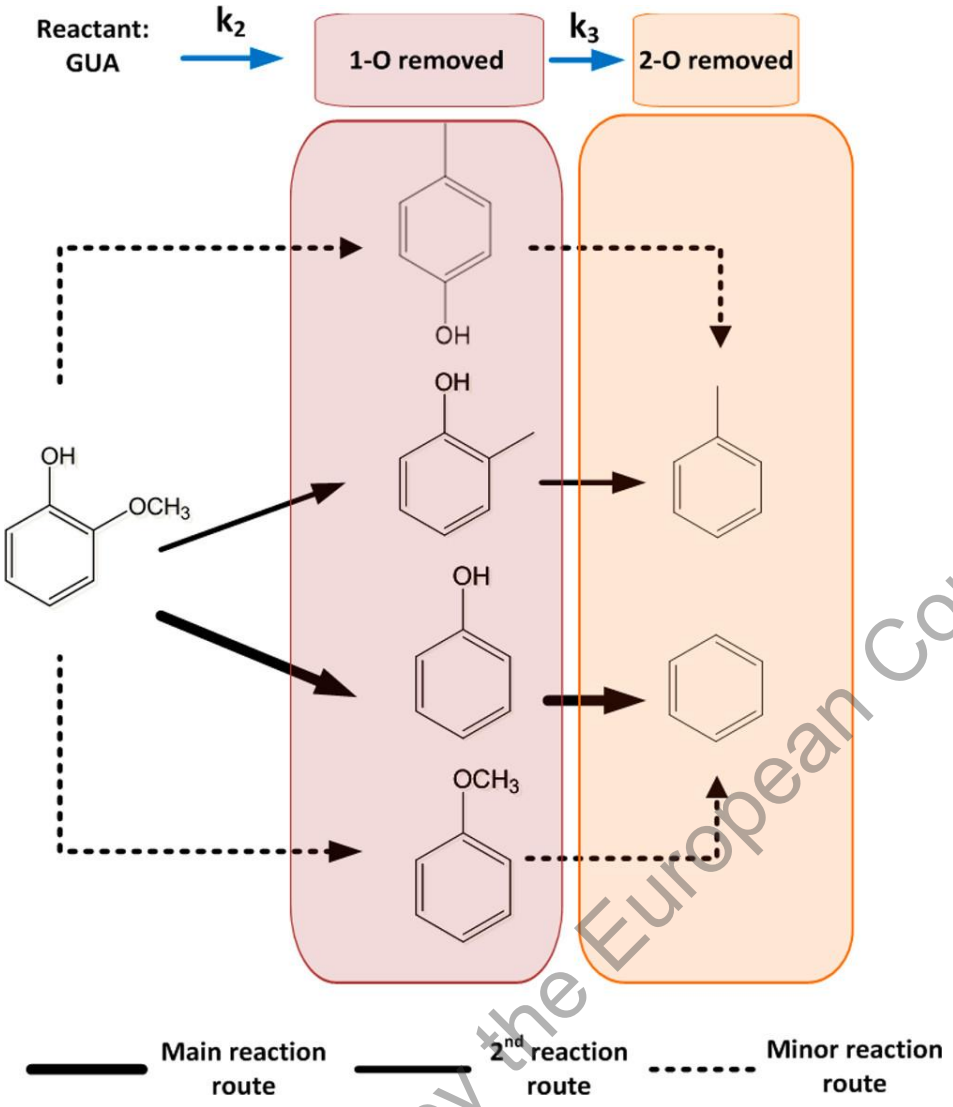

Figure 29. A proposed reaction network for guaiacol HDO via Mo_2C/AC catalyst. (Liu et al., 2017)

In Figure 27, reactions were grouped into aliphatic hydrogenated products (HYD), deoxygenated products with one O-atom removed (1-O removed) and deoxygenated products with two O-atoms removed (2-O removed). The ordinary differential equations (ODEs) derived by Liu et al. (2017) for the reaction network of Pd/AC are shown in Equation 10 - Equation 13.

Equation 10

$$\frac{dC_{GUA}}{dt} = -k_1 C_{GUA}$$

Equation 11

$$\frac{dC_{HYD}}{dt} = k_1 C_{GUA} - k_2 C_{HYD}$$

Equation 12

$$\frac{dC_{1-O}}{dt} = k_2 C_{HYD} - k_3 C_{1-O}$$

Equation 13

$$\frac{dC_{2-O}}{dt} = k_3 C_{1-O}$$

, where C_{GUA} is the concentration of guaiacol, C_{HYD} is the concentration of the aliphatic products, C_{1-O} is the concentration of products with one O-atom removed and C_{2-O} is the concentration of products with both O-atoms removed. The authors used Levenberg-Marquardt nonlinear methodology along with Runge-Kutta numerical integration to solve the ODEs and estimate the values of the reaction rate constants. The same methodology for solving the ODEs was used in the Ru/AC and Mo_2C/AC reaction networks. In Figure 28, in addition to the three groups of compounds used in Figure 27, a fourth group was introduced for the fully deoxygenated products that were alkylated. Thus, a modified version of Equation 13 was used and an additional equation besides the existing Equation 10 - Equation 12 was derived. They are shown in Equation 14 and Equation 15.

Equation 14

$$\frac{dC_{2-O}}{dt} = k_3 C_{1-O} - k_4 C_{2-O}$$

Equation 15

$$\frac{dC_{Alk}}{dt} = k_4 C_{2-O}$$

, where C_{Alk} is the concentration of the fully deoxygenated alkylated products. In Figure 29 (HDO over Mo_2C/AC catalyst) there were only two groups of compounds, which represent the deoxygenated products without alkylation. Slightly altered ODEs were thus used by the authors shown in Equation 16 - Equation 18.

Equation 16

$$\frac{dC_{GUA}}{dt} = -k_2 C_{GUA}$$

Equation 17

$$\frac{dC_{1-O}}{dt} = k_2 C_{GUA} - k_3 C_{1-O}$$

Equation 18

$$\frac{dC_{2-O}}{dt} = k_3 C_{1-O}$$

Liu et al. (2017) reported signs of temperature dependency in all three reaction networks. The calculated activation energies for the HDO via Pd/AC were $38 \pm 2 \frac{kJ}{mol}$, $146 \frac{kJ}{mol}$ and $121 \frac{kJ}{mol}$ for the hydrogenation, first deoxygenation and second deoxygenation step respectively. For the Ru/AC catalyst, the calculated activation energies were $40 \pm 6 \frac{kJ}{mol}$, $68 \pm 1 \frac{kJ}{mol}$ and $110 \pm 25 \frac{kJ}{mol}$ for the hydrogenation, first deoxygenation and second deoxygenation step respectively. No activation energy was calculated for the alkylation step. The activation energies of the first and second deoxygenation step for Mo_2C/AC were $83 \pm 3 \frac{kJ}{mol}$ and $151 \pm 8 \frac{kJ}{mol}$ respectively. In

the HDO via Pd/AC, the amount of hydrogenated products decreased with increasing temperature, while the deoxygenated products increased with increasing temperature. The same was observed for Ru/AC, with the addition of alkylated products also increasing with higher temperatures. For Mo_2C/AC only deoxygenated products were detected at 603 K with increasing temperatures decreasing the amount of products with one O-atom removed and increasing the fully deoxygenated products.

The reaction rate constants that Liu et al. (2017) calculated for the oxygen removal and alkylation steps for all three catalysts were lower than the reaction rate of the hydrogenation. Conversely, the apparent activation energies for the oxygen removal steps were higher than the apparent activation energy of the hydrogenation step.

Figure 29 is significantly different from Figure 27 and Figure 28, since no hydrogenation of the aromatic ring is present. This might support the previous discussions in this deliverable report by confirming that different catalysts might affect the HDO reaction so drastically that some intermediate compounds would exist only when using certain specific catalysts. It should however be noted that the experiments done using Mo_2C/AC were performed at 603 – 648 K, whereas for the other two catalysts, 603 K was the maximum temperature in which they were used. At temperatures lower than 573 K there were still products that had undergone hydrogenation of the aromatic ring while still retaining both oxygen containing functional groups. At 603 K the product distributions of both Pd/AC and Ru/AC only contained deoxygenated products. Thus, to truly verify the accuracy of the reaction pathways of Figure 29, the experiments would need to be done in the complete same temperature range as with the other two catalysts.

The reaction network depicted in Figure 27 is fairly similar to the ones proposed by Zhao et al. (2011) and Zhang et al. (2016), with some differences in the intermediate products. The experimental temperatures and pressures were comparable, with slight differences in the catalyst. Thus, the most likely contributors to the differences between the reaction networks were the bi-functional catalysts used by Zhao et al. (2011) and Zhang et al. (2016) and the hydrothermal/aqueous conditions.

2.2.3 Non-hydrothermal HDO of benzofuran

Yang et al. (2021) also studied the HDO of benzofuran. The reaction network proposed by the authors is shown in Figure 30. Comparing this reaction network to the one proposed by Dickinson et al. (2012) shown in Figure 15, there are several differences. The reaction networks start diverging at ethylphenol, which is not present in Figure 30. The upper path shown in Figure 30 does not exist in Figure 15, and although the final product of the lower path in Figure 30, ethyl cyclohexane, is present in both figures, the reaction networks contain different intermediates.

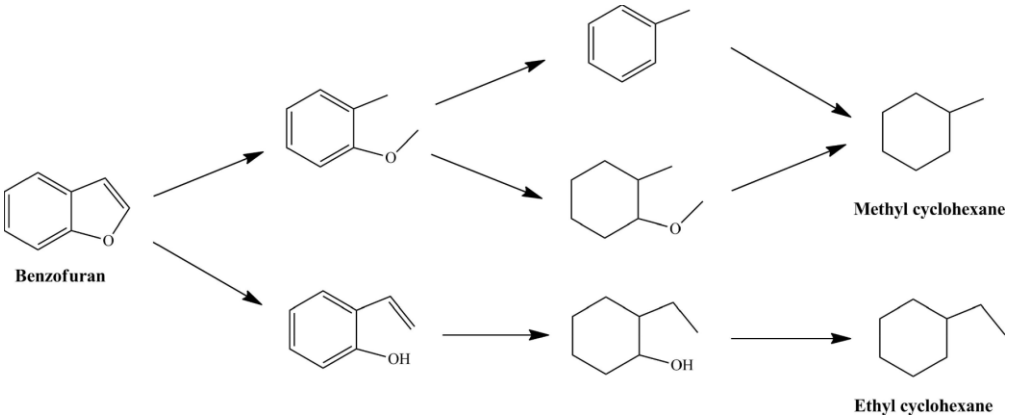

Figure 30. A proposed reaction pathway for benzofuran using Ru/C and H_2WO_4. (Yang et al., 2021)

The reason for the differences between Figure 30 and Figure 15 could be due to the different conditions imposed in both studies. Significant differences include the aqueous-phase HDO and use of supercritical water by Dickinson et al. (2012) in addition to the different catalysts used. There was also a difference in the reaction temperatures, which in the case of phenols, could affect the observed reaction network. However, neither Dickinson et al. (2012) nor Yang et al. (2021) discuss any temperature dependence for the HDO of benzofurans and since the temperatures used in both studies are somewhat comparable, it can be assumed that temperature is not a significant contributor the differences in the reaction networks. The kinetic studies on phenolic compounds show that for the complete reaction, both metallic and acidic functions of the catalysts are required. While this was not studied by Dickinson et al. (2012) nor Yang et al. (2021), it could explain the key differences, and if not, then this could indicate that performing the HDO process in an aqueous-phase or using supercritical water affects the kinetics of the overall process.

Bunch et al. (2002) studied the kinetics of benzofuran HDO. The experiments were done in a fixed-bed reactor using sulphided and reduced NiMo/γ-Al_2O_3 catalysts. The experimental conditions were 393 – 633 K and 2,17 – 5,62 MPa. Other reactants besides benzofuran were also used. These were 2,3-dihydrobenzofuran, 2-ethylphenol and 2-ethylcyclohexanol. Based on the results of the experiments, the authors proposed two reaction networks for the HDO of benzofuran over sulphided and reduced catalysts. The reaction network for the sulphided catalysts is shown in Figure 31. The first two steps shown in Figure 31 were determined to be a hydrogenation step, followed by hydrogenolysis. The third step reacted differently to the addition of H_2S compared to the second step, which led the authors to believe that the conversion of EP must then happen through something other than direct hydrogenolysis. The authors suspect that there is an undetected intermediate between EP and EB that is produced from the hydrogenation of EP. The intermediate DHEP could then be converted to EB through an E2 Hoffman-type elimination reaction.

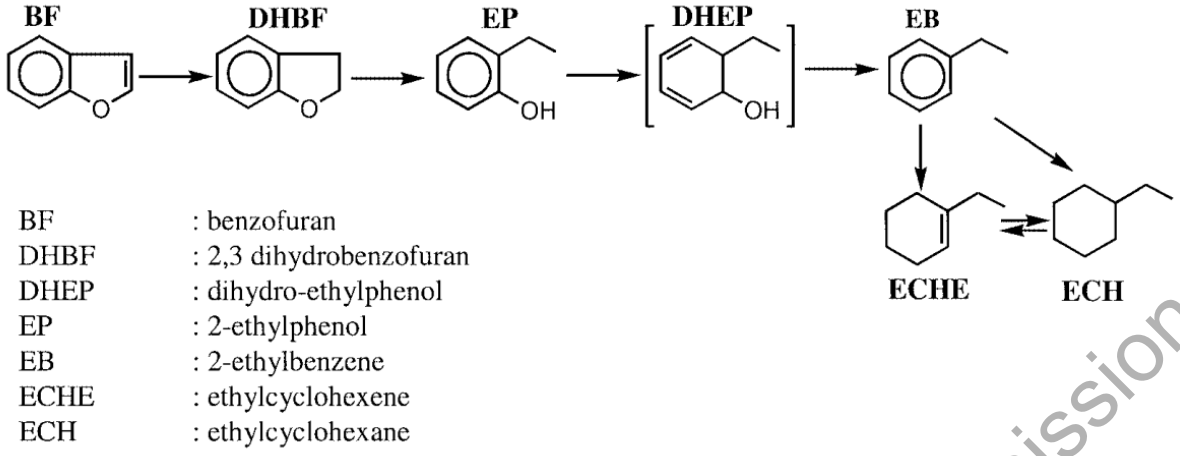

Figure 31. A proposed reaction network for the HDO of benzofuran via sulphided Ni-Mo catalysts. (Bunch & Ozkan, 2002)

The reaction network of the reduced catalysts by Bunch et al. (2002) is shown in Figure 32. When using the reduced catalyst, the authors detected additional oxygen containing intermediates that were not present with the sulphided catalyst. The authors added a secondary route for ECHE and ECH formation through the saturation of the aromatic ring in DHBF. The hydrogenation activity of the reduced catalyst was found to be higher than the sulphided catalyst. This was demonstrated by the lack of EP formation when using the reduced catalysts, where the reaction proceeded mainly through the hydrogenation of the aromatic ring in DHBF. Another difference between the catalysts that the authors have highlighted was the higher reactivity of the oxygen containing intermediates compared to EP. While EP could not directly undergo S_N2 nucleophilic substitution or an E2 Hoffman type elimination reaction, both were possible on the oxygen containing intermediates on the reduced catalyst with the addition of direct cleavage. While the authors believe that under certain conditions the reaction network shown in Figure 32 could have reversible steps, they were considered to be irreversible in respect to the experimental conditions used. This was based on the observations when using EP and DHBF as the reactants. When using EP, no DHBF was formed and when using DHBF, no BF was formed.

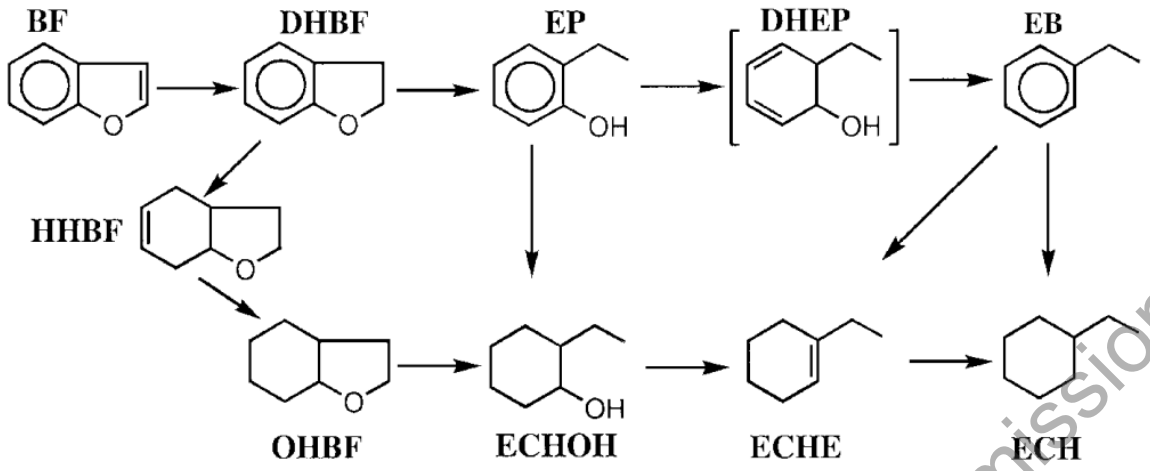

BF	: benzofuran	ECHOH	: ethylcyclohexanol
DHBF	: 2,3 dihydrobenzofuran	DHEP	: dihydro-ethylphenol
HHBF	: hexahydrobenzofuran	ECH	: ethylcyclohexane
OHBF	: octahydrobenzofuran	EB	: ethylbenzene
EP	: 2-ethylphenol	ECHE	: ethylcyclohexene

Figure 32. A proposed reaction network for the HDO of benzofuran via reduced Ni-Mo catalysts. (Bunch & Ozkan, 2002)

When comparing the two reaction networks proposed by Bunch et al. (2002) to the hydrothermal one shown in Figure 15, both are quite similar. Figure 15 contains mostly the same intermediates shown in Figure 31 except ECHE and DHEP, although DHEP was also undetected by Bunch et al. (2002). Figure 15 does not contain all the additional oxygen containing intermediates shown in Figure 32, but both figures do depict the conversion of EP to ECHOH. This could be due to the different catalysts used or the experimental conditions including the hydrothermal conditions used by Dickinson et al. (2012).

Romero et al. (2009) studied the kinetics of benzofuran HDO via a sulphided NiMoP/Al_2O_3 catalyst. The experiments were done in a fixed-bed reactor and toluene was used as a solvent. The experimental conditions were 613 K and 7 MPa total pressure. To better determine the reaction network the authors also used 2,3-dihydrobenzofuran and 2-ethylphenol as reagents. The authors proposed a reaction network for benzofuran which is shown in Figure 33. Like in the previously discussed study by Romero et al. (2010) in this deliverable report, the reaction network in Figure 33 is shown to have three pathways. These are the hydrogenation route, direct deoxygenation route and the route that is created from the interactions with the acidic properties of the catalyst. Romero et al. (2009) found that the hydrogenation route was the primary route in the reaction. Compared to the reaction network proposed by Dickinson et al. (2012) shown in Figure 15 the DDO and HYD paths in Figure 33 are relatively similar except for some intermediates. The major differences are present in the ACI path in Figure 33. Of all the compounds shown in the ACI path, only phenol is shown in Figure 15. This is likely due to Dickinson et al. (2012) using a Pt/C catalyst, while Romero et al. (2009) used a sulphided NiMoP/Al_2O_3 catalyst. Both the active metals and the support are different which can contribute

to the differences in the reaction networks. This especially applies to the support, since the ACI path was identified by Romero et al. (2009) to be closely related to the acidic interactions with the catalyst support. The effects of the hydrothermal conditions used in Dickinson et al. (2012) on the reaction network is difficult to determine since there were many other factors to also be accounted for.

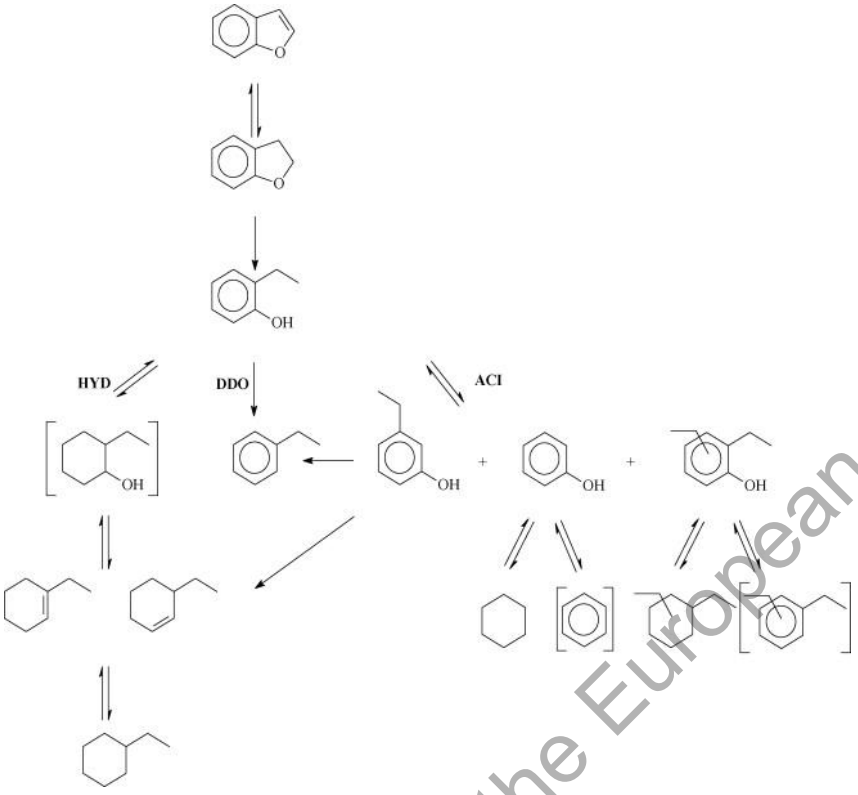

Figure 33. A proposed reaction network for benzofuran HDO via NiMoP/Al_2O_3 catalyst. The brackets indicate compounds that were not detected. (Romero et al., 2009)

3 Conclusions

In this work, the kinetics of hydrothermal and non-hydrothermal HDO was discussed by reviewing available literature. Proposed reaction networks were compared with each other to evaluate different factors that could affect the kinetics such as reaction temperature. Additionally, some methodologies used for evaluating the kinetic parameters were also presented alongside calculated activation energies.

Regardless of the catalysts used in hydrothermal HDO of phenols, the studies indicate that cycloalkanes and cycloalkanols are the main products. Most of the studies agreed that the reactions begin with the hydrogenation of the aromatic ring. The true contribution of the hydrothermal/aqueous phase on the kinetics of HDO was difficult to determine, since for some of the studies, the aqueous phase was used to introduce a homogeneous acid into the reaction. The use of acid seems to alter the reaction networks, indicating that certain reaction steps are acid-catalyzed. For the studies where acid was not used, the hydrogenation of the aromatic rings happened later in the reaction network as opposed to earlier. Most studies noted a temperature dependence in the reaction where the formation of cycloalkanes required a certain temperature. The temperature dependence might indicate that the last steps of the reaction have higher activation energies. Based on the calculations of the studies presented in this deliverable report, the activation energies for the different reaction steps range from about 30 $\frac{kJ}{mol}$ up to 150 $\frac{kJ}{mol}$. It should however be noted that different phenolic compounds and catalysts were used between the studies, which could affect the calculated values. Thus, the calculated values might not be comparable. There were significantly less studies found for the hydrothermal HDO of benzofuran. Based on the one study that was found, it seems that both cycloalkanes and benzenes are produced.

Compared to the hydrothermal HDO of phenols, there seemed to be more variation between the reaction networks of non-hydrothermal HDO of phenols. Some studies showed the hydrogenation of the aromatic ring happening at the beginning of the reaction network while others placed it near the end. The difference might be explained by low hydrogen pressure used in the experiments, since in some of the studies where hydrogenation of the aromatic ring was observed to happen later on, the pressure was significantly lower than in most of the other studies. Otherwise, the reaction networks had similar structures as those presented in chapter 2.1, with differences mostly related to the intermediate species.

From the studies shown in this work regarding benzofuran, they indicate that the reaction networks mainly consist of aromatic compounds, where the hydrogenation of the aromatic ring happens later in the reaction. All the studies also contain one route where the hydrogenation of the aromatic ring happens earlier. Similarly to the phenols, the reaction networks were generally the same as in chapter 2.1 and the differences could not be completely attributed to the hydrothermal environment. Compared to the phenols however, the comparisons made for benzofuran are less reliable as for this deliverable report only one study on the hydrothermal HDO of benzofuran was found.

When comparing to the studies in chapter 2.1, it was difficult to evaluate the effect that the hydrothermal environment had on the kinetics of HDO since in many of the studies there were some factors that differed. Another aspect that hindered the comparisons was that most studies focused on phenols and benzofurans, while real oils and other model components are used less often. Based on the two kinetics studies found that used real oils, it seems that while some of the steps in the reaction networks are the same, the overall distribution of products is quite different compared to the studies using model components. Little cycloalkanes and cycloalkanols are detected in the products with the distribution having a broader range of components in general. Though it should be noted that the distribution also depends on the quality of the oil being upgraded. In the study by Sanna et a. (2015), two major components in the feed were levoglucosan and hydroxyacetaldehyde followed by catechol which would naturally produce a wider range of components than just the HDO of phenols. Lastly, from the studies presented in this deliverable report, there does not seem to be major differences in the reaction networks of hydrothermal and non-hydrothermal HDO that could be solely attributed to the hydrothermal environment, although this may be restricted only to the reactions involving phenols and benzofurans. When observing the studies presented in Chapter 2.2, it seems that the choice of catalyst might have a larger effect on the reaction network than the use of water, though more experimental work will still be needed to verify this claim.

4 Bibliography

Bunch, A. Y., & Ozkan, U. S. (2002). Investigation of the Reaction Network of Benzofuran Hydrodeoxygenation over Sulfided and Reduced Ni–Mo/Al2O3 Catalysts. *Journal of Catalysis*, *206*(2), 177-187. https://doi.org/https://doi.org/10.1006/jcat.2001.3490

Dickinson, J. G., Poberezny, J. T., & Savage, P. E. (2012). Deoxygenation of benzofuran in supercritical water over a platinum catalyst. *Applied Catalysis B: Environmental*, *123-124*, 357-366. https://doi.org/https://doi.org/10.1016/j.apcatb.2012.05.005

Hellinger, M., Carvalho, H. W. P., Baier, S., Wang, D., Kleist, W., & Grunwaldt, J.-D. (2015). Catalytic hydrodeoxygenation of guaiacol over platinum supported on metal oxides and zeolites. *Applied Catalysis A: General*, *490*, 181-192. https://doi.org/https://doi.org/10.1016/j.apcata.2014.10.043

Infantes-Molina, A., Gralberg, E., Cecilia, J. A., Finocchio, E., & Rodríguez-Castellón, E. (2015). Nickel and cobalt phosphides as effective catalysts for oxygen removal of dibenzofuran: role of contact time, hydrogen pressure and hydrogen/feed molar ratio [10.1039/C5CY00282F]. *Catalysis Science & Technology*, *5*(6), 3403-3415. https://doi.org/10.1039/C5CY00282F

Kruse, A., & Dinjus, E. (2007). Hot compressed water as reaction medium and reactant: Properties and synthesis reactions. *The Journal of Supercritical Fluids*, *39*(3), 362-380. https://doi.org/https://doi.org/10.1016/j.supflu.2006.03.016

Lee, H., Kim, H., Yu, M. J., Ko, C. H., Jeon, J.-K., Jae, J., Park, S. H., Jung, S.-C., & Park, Y.-K. (2016). Catalytic Hydrodeoxygenation of Bio-oil Model Compounds over Pt/HY Catalyst. *Scientific Reports*, *6*(1), 28765. https://doi.org/10.1038/srep28765

Lin, Y.-C., Li, C.-L., Wan, H.-P., Lee, H.-T., & Liu, C.-F. (2011). Catalytic Hydrodeoxygenation of Guaiacol on Rh-Based and Sulfided CoMo and NiMo Catalysts. *Energy & Fuels*, *25*(3), 890-896. https://doi.org/10.1021/ef101521z

Liu, S., Wang, H., Smith, K. J., & Kim, C. S. (2017). Hydrodeoxygenation of 2-Methoxyphenol over Ru, Pd, and Mo2C Catalysts Supported on Carbon. *Energy & Fuels*, *31*(6), 6378-6388. https://doi.org/10.1021/acs.energyfuels.7b00452

Liu, X., Guo, Y., Xu, D., & Guan, Q. (2022). A review on recent advances in clean microalgal bio-oil production via catalytic hydrothermal deoxygenation. *Journal of Cleaner Production*, *366*, 132978. https://doi.org/https://doi.org/10.1016/j.jclepro.2022.132978

Nelson, R. C., Baek, B., Ruiz, P., Goundie, B., Brooks, A., Wheeler, M. C., Frederick, B. G., Grabow, L. C., & Austin, R. N. (2015). Experimental and Theoretical Insights into the Hydrogen-Efficient Direct Hydrodeoxygenation Mechanism of Phenol over Ru/TiO2. *ACS Catalysis*, *5*(11), 6509-6523. https://doi.org/10.1021/acscatal.5b01554

Nimmanwudipong, T., Runnebaum, R. C., Block, D. E., & Gates, B. C. (2011). Catalytic Conversion of Guaiacol Catalyzed by Platinum Supported on Alumina: Reaction Network Including Hydrodeoxygenation Reactions. *Energy & Fuels*, *25*(8), 3417-3427. https://doi.org/10.1021/ef200803d

Oh, S., Hwang, H., Choi, H. S., & Choi, J. W. (2015). The effects of noble metal catalysts on the bio-oil quality during the hydrodeoxygenative upgrading process. *Fuel*, *153*, 535-543. https://doi.org/https://doi.org/10.1016/j.fuel.2015.03.030

Romero, Y., Richard, F., & Brunet, S. (2010). Hydrodeoxygenation of 2-ethylphenol as a model compound of bio-crude over sulfided Mo-based catalysts: Promoting effect and reaction mechanism. *Applied Catalysis B: Environmental*, *98*(3), 213-223. https://doi.org/https://doi.org/10.1016/j.apcatb.2010.05.031

Romero, Y., Richard, F., Renème, Y., & Brunet, S. (2009). Hydrodeoxygenation of benzofuran and its oxygenated derivatives (2,3-dihydrobenzofuran and 2-ethylphenol) over NiMoP/Al2O3 catalyst. *Applied Catalysis A: General*, *353*(1), 46-53. https://doi.org/https://doi.org/10.1016/j.apcata.2008.10.022

Saidi, M., & Safaripour, M. (2022). Aqueous phase hydrodeoxygenation of anisole as a pyrolysis lignin-derived bio-oil by ether-functionalized ionic polymer-stabilized Ni-Mo nanocatalyst. *Sustainable Energy Technologies and Assessments*, *49*, 101770. https://doi.org/https://doi.org/10.1016/j.seta.2021.101770

Sanna, A., Vispute, T. P., & Huber, G. W. (2015). Hydrodeoxygenation of the aqueous fraction of bio-oil with Ru/C and Pt/C catalysts. *Applied Catalysis B: Environmental*, *165*, 446-456. https://doi.org/https://doi.org/10.1016/j.apcatb.2014.10.013

Şenol, O. İ., Ryymin, E. M., Viljava, T. R., & Krause, A. O. I. (2007). Effect of hydrogen sulphide on the hydrodeoxygenation of aromatic and aliphatic oxygenates on sulphided catalysts. *Journal of Molecular Catalysis A: Chemical*, *277*(1), 107-112. https://doi.org/https://doi.org/10.1016/j.molcata.2007.07.033

Yang, J., Williams, C. L., Ramasubramaniam, A., & Dauenhauer, P. J. (2014). Aqueous-phase hydrodeoxygenation of highly oxygenated aromatics on platinum [10.1039/C3GC41138A]. *Green Chemistry*, *16*(2), 675-682. https://doi.org/10.1039/C3GC41138A

Yang, Z., Luo, B., Shu, R., Tian, Z., Kang, Y., & Chen, Y. (2021). Efficient hydrodeoxygenation of phenolic compounds and raw lignin-oil under a temperature-controlled phase-transfer catalysis. *Fuel*, *291*, 120091. https://doi.org/https://doi.org/10.1016/j.fuel.2020.120091

Yu, Z., Wang, Y., Liu, S., Yao, Y., Sun, Z., Li, X., Liu, Y., Wang, W., Wang, A., Camaioni, D. M., & Lercher, J. A. (2018). Aqueous Phase Hydrodeoxygenation of Phenol over Ni3P-CePO4 Catalysts. *Industrial & Engineering Chemistry Research*, *57*(31), 10216-10225. https://doi.org/10.1021/acs.iecr.8b01606

Yu, Z., Wang, Y., Sun, Z., Li, X., Wang, A., Camaioni, D. M., & Lercher, J. A. (2018). Ni3P as a high-performance catalytic phase for the hydrodeoxygenation of phenolic compounds [10.1039/C7GC03262E]. *Green Chemistry*, *20*(3), 609-619. https://doi.org/10.1039/C7GC03262E

Zhang, C., Qi, J., Xing, J., Tang, S.-F., Song, L., Sun, Y., Zhang, C., Xin, H., & Li, X. (2016). An investigation on the aqueous-phase hydrodeoxygenation of various methoxy-substituted lignin monomers on Pd/C and HZSM-5 catalysts [10.1039/C6RA22492J]. *RSC Advances*, *6*(106), 104398-104406. https://doi.org/10.1039/C6RA22492J

Zhao, C., He, J., Lemonidou, A. A., Li, X., & Lercher, J. A. (2011). Aqueous-phase hydrodeoxygenation of bio-derived phenols to cycloalkanes. *Journal of Catalysis*, *280*(1), 8-16. https://doi.org/https://doi.org/10.1016/j.jcat.2011.02.001

Zhao, C., Kou, Y., Lemonidou, A. A., Li, X., & Lercher, J. A. (2009). Highly Selective Catalytic Conversion of Phenolic Bio-Oil to Alkanes. *Angewandte Chemie International Edition*, *48*(22), 3987-3990. https://doi.org/https://doi.org/10.1002/anie.200900404